OULU 2013
D 1198

ACTA UNIVERSITATIS OULUENSIS

Janne Koivumäki

BIOMECHANICAL MODELING OF PROXIMAL FEMUR

DEVELOPMENT OF FINITE ELEMENT MODELS TO SIMULATE FRACTURES

UNIVERSITY OF OULU GRADUATE SCHOOL;
UNIVERSITY OF OULU,
FACULTY OF MEDICINE,
INSTITUTE OF BIOMEDICINE,
DEPARTMENT OF MEDICAL TECHNOLOGY

ACTA UNIVERSITATIS OULUENSIS
D Medica 1198

JANNE KOIVUMÄKI

BIOMECHANICAL MODELING OF PROXIMAL FEMUR

Development of finite element models to simulate fractures

Academic dissertation to be presented with the assent of the Doctoral Training Committee of Health and Biosciences of the University of Oulu for public defence in Auditorium A101 of the Department of Anatomy and Cell Biology (Aapistie 7 A), on 15 March 2013, at 12 noon

UNIVERSITY OF OULU, OULU 2013

Acta Univ. Oul. D 1198, 2013

Supervised by
Professor Timo Jämsä

Reviewed by
Professor Peter Augat
Professor Mark Taylor

ISBN 978-952-62-0090-3 (Paperback)
ISBN 978-952-62-0091-0 (PDF)

ISSN 0355-3221 (Printed)
ISSN 1796-2234 (Online)

Cover Design
Raimo Ahonen

JUVENES PRINT
TAMPERE 2013

Koivumäki, Janne, Biomechanical modeling of proximal femur. Development of finite element models to simulate fractures

University of Oulu Graduate School; University of Oulu, Faculty of Medicine, Institute of Biomedicine, Department of Medical Technology, P.O. Box 5000, FI-90014 University of Oulu, Finland

Acta Univ. Oul. D 1198, 2013
Oulu, Finland

Abstract

Hip fracture is a significant problem in health care incurring major costs to society. Therefore, it is necessary to study fracture mechanisms and develop improved methods to estimate individual fracture risk. In addition to conventional bone density measurements, computational finite element (FE) analysis has been recognized as a valuable method for studying biomechanical characteristics of a hip fracture.

In this study, computed tomography (CT) based finite element methods were investigated and simulation models were developed to estimate experimental femoral fracture load and hip fracture type in a sideways fall loading configuration. Cadaver femur specimens (age 55–100 years) were scanned using a CT scanner and dual-energy X-ray absorptiometry (DXA), and the femurs were mechanically tested for failure in a sideways fall loading configuration. CT images were used for generating the FE model, and DXA was used as a reference method. FE analysis was done for simulation models of the proximal femur in a sideways fall loading configuration to estimate the experimentally measured fracture load and fracture type. Statistical analyses were computed to compare the experimental and the FE data.

Cervical and trochanteric hip fractures displayed characteristic strain patterns when using a FE model mainly driven by bone geometry. This relatively simple FE model estimation provided reasonable agreement for the occurrence of experimental hip fracture type. Accurate assessment between experimental and finite element fracture load ($r^2 = 0.87$) was achieved using subject-specific modeling, including individual material properties of trabecular bone for bilinear elastoplastic FE models. Nevertheless, the study also showed that proximal femoral fracture load can be estimated with reasonable accuracy ($r^2 = 0.73$) by a relatively simple FE model including only cortical bone. The cortical bone FE model was more predictive for fracture load than DXA and slightly less accurate than the subject-specific FE model. The accuracy and short calculation time of the model suggest promise in terms of effective clinical use.

Keywords: biomechanics, cervical fracture, computed tomography, femoral neck, finite element, fracture load, fracture risk, hip fracture, trochanteric fracture

Koivumäki, Janne, Reisiluun biomekaaninen mallintaminen. Simulointimallien kehittäminen lonkkamurtuman arviointiin
Oulun yliopiston tutkijakoulu; Oulun yliopisto, Lääketieteellinen tiedekunta, Biolääketieteen laitos, Lääketieteen tekniikka, PL 5000, 90014 Oulun yliopisto
Acta Univ. Oul. D 1198, 2013
Oulu

Tiivistelmä

Lonkkamurtuma on huomattava ongelma terveydenhuollossa aiheuttaen merkittäviä kustannuksia yhteiskunnalle. Tämän vuoksi on tärkeää tutkia ja kehittää uusia yksilöllisen murtumariskin arviointimenetelmiä. Elementtimenetelmä on tehokas laskennallinen työkalu lonkkamurtuman biomekaanisten ominaisuuksien tutkimisessa.

Tässä työssä tutkittiin ja kehitettiin tietokonetomografiaan perustuvia reisiluun simulaatiomalleja kokeellisten murtolujuuksien ja lonkkamurtumatyyppien arviointiin. Reisiluunäytteet (ikä 55–100 vuotta) kuvattiin tietokonetomografialaitteella ja kaksienergisellä röntgenabsorptiometrialla, jonka jälkeen reisiluut kuormitettiin kokeellisesti murtolujuuden ja murtumatyypin määrittämiseksi sivuttaiskaatumisasetelmassa. Tietokonetomografialeikekuvia käytettiin simulaatiomallien luomiseen, ja kaksienergistä röntgenabsorptiometriaa käytettiin vertailumenetelmänä. Reisiluun simulaatiomallit analysoitiin elementtimenetelmän avulla kokeellisten murtolujuuksien ja murtumatyyppien arvioimiseksi. Tilastoanalyysiä käytettiin verrattaessa kokeellista aineistoa ja simulaatioaineistoa.

Reisiluun muotoon perustuva simulaatiomalli osoitti, että reisiluun kaulan ja sarvennoisen murtumilla on tyypilliset jännitysjakaumat. Tämän suhteellisen yksinkertaisen mallin murtumatyyppi oli lähes yhdenmukainen kokeellisen murtumatyypin kanssa. Reisiluun kokeellinen murtolujuus pystyttiin arvioimaan tarkasti (r^2 = 0.87) käyttäen yksityiskohtaista simulaatiomallia, joka sisältää yksilölliset hohkaluun materiaaliominaisuudet. Toisaalta murtolujuus pystyttiin arvioimaan kohtuullisella tarkkuudella (r^2 = 0.73) melko yksinkertaisellakin mallilla, joka käsittää ainoastaan kuoriluun. Kuoriluuhun perustuva malli oli tarkempi arvioimaan reisiluun kokeellista murtolujuutta kuin kaksienerginen röntgenabsorptiometria ja lähes yhtä tarkka kuin yksityiskohtaisempi simulaatiomalli. Mallin tarkkuus ja lyhyt laskenta-aika antavat lupauksia tehokkaaseen kliiniseen käyttöön.

Asiasanat: biomekaniikka, finite element, lonkkamurtuma, murtolujuus, murtumariski, reisiluu, reisiluun kaulan murtuma, sarvennoismurtuma, tietokonetomografia

To my family

Acknowledgements

This study was carried out at the Institute of Biomedicine, Department of Medical Technology, at the University of Oulu during the years 2008–2013. The research was partly done as telework. I wish to thank my supervisor, Professor Timo Jämsä, for giving me the opportunity to join this project, and for his guidance and support throughout these years.

I want to thank my other co-authors at the department, PhD Jérôme Thevenot and PhD Pasi Pulkkinen, for their contribution to this thesis. Jérôme, I am grateful for our close co-operation during the past few years, the productive conversations we have had, and for the modeling support. Pasi, I greatly appreciate your statistical advice and the interesting scientific aspects that you have brought out in our conversations over the years.

I wish to express my gratitude to the co-authors, Prof. Felix Eckstein, Prof. Thomas Link, MD Volker Kuhn, and MD Eva-Maria Lochmüller. Thank you for the treasured experimental material. I especially want to thank Felix Eckstein and Thomas Link for their valuable comments and constructive criticism during the study. Co-author MSc Jukka Salmi is acknowledged for his scientific initiative.

I am very grateful to the official reviewers of this thesis, Prof. Peter Augat and Prof. Mark Taylor, for their valuable comments and revisions of the manuscript. I also wish to thank Anna Vuolteenaho for revision of the language.

I want to thank Prof. Miika Nieminen for his useful comments and for arranging the segmentation facilities. Researcher Risto Bloigu is acknowledged for statistical consultation.

I would like to thank the staff of the Department of Medical Technology. Thank you for your company and support. Special thanks to Mikko Finnilä for the cultural insights on our joint business trips.

Above all, my deepest gratitude and love goes to my family, my wife Stiina and our daughter Anna-Sofia. Stiina, you have been understanding, encouraging and supportive during this whole project, even though my thoughts often wander around work at home. Thank you for your love and support during the years, and for taking care of your family. Anna-Sofia, you brighten my every day, and your smile makes me forget my worries. Thank you for bringing us so much happiness.

I wish to express my warmest gratitude to my mum and dad, and my sisters for their love and support throughout my life. I also want to thank my parents-in-law for their help and support, and my friends and relatives for their interest in my work.

I want to thank CSC - IT Center for Science Ltd. for providing software and computational assistance. This study was funded by the Finnish Funding Agency for Technology and Innovation, the National Doctoral Programme of Musculoskeletal Disorders and Biomaterials, and the Finnish Cultural Foundation, North Ostrobothnia Regional fund. I express my gratitude for the support.

Abbreviations and symbols

Δ	difference of two values
α	material constant
ε	strain
ε_C	cervical principal strain
ε_C	principal strain in compression
ε_T	trochanteric principal strain
$\mu\varepsilon$	microstrain
μCT	micro-computed tomography
ρ	equivalent computed tomography density
ρ_{ash}	ash density
σ	stress
σ_m	mean stress
σ_T	principal stress in tension
σ_{yc}	yield stress for cortical bone
σ_{VM}	von Mises stress
σ_{yt}	yield stress for trabecular bone
ANCOVA	analysis of covariance
AO	Arbeitsgemeinschaft für Osteosynthesefragen
BMC	bone mineral content
BMD	bone mineral density
BMI	body mass index
BMU	basic multicellular unit
BRU	bone remodeling unit
CI	confidence interval
CSA	cross-sectional area
CT	computed tomography
DXA	dual-energy X-ray absorptiometry
E	Young's modulus
F	global nodal force
F	female
FE	finite element
FNAL	femoral neck axis length
FNBMD	femoral neck bone mineral density
FRAX^{TM}	WHO Fracture Risk Assessment Tool
HAL	hip axis length

K	global stiffness matrix
k	Drucker-Prager yield strength
l	length
M	male
m	median
MD-CT	multi-detector computed tomography
MES	minimum effective strain
MRI	magnetic resonance imaging
NSA	femoral neck-shaft angle
N	number of samples
p	p-value for statistical significance
pQCT	peripheral quantitative computed tomography
QCT	quantitative computed tomography
r	correlation coefficient
r^2	coefficient of determination
ROC	receiver operating characteristic
SD	standard deviation
SEE	standard error of estimate
SR-CT	synchrotron computed tomography
TRBMD	trochanteric bone mineral density
U	global nodal displacement
US	ultrasound
VXA	volumetric dual-energy X-ray absorptiometry
WHO	World Health Organization

List of original publications

This thesis is based on three original articles that are referred to in the text by their Roman numerals (I–III):

I Koivumäki J, Thevenot J, Pulkkinen P, Salmi J, Kuhn V, Lochmüller E-M, Link T, Eckstein F & Jämsä T (2010) Does femoral strain distribution coincide with the occurrence of cervical versus trochanteric hip fractures? - An experimental finite element study. Med Biol Eng Comput 48(7): 711–717.

II Koivumäki J, Thevenot J, Pulkkinen P, Kuhn V, Link T, Eckstein F & Jämsä T (2012) CT-based finite element models can be used to estimate experimentally measured failure loads in the proximal femur. Bone 50(4): 824–829.

III Koivumäki J, Thevenot J, Pulkkinen P, Kuhn V, Link T, Eckstein F & Jämsä T (2012) Cortical bone finite element models in the estimation of experimentally measured failure loads in the proximal femur. Bone 51(4): 737–740.

Contents

1 Introduction

Hip fracture is a significant problem in health care incurring major costs to society, and at worst, causing morbidity and mortality among the elderly. In Finland, it has been estimated that the average 1-year cost of a patient with a hip fracture is over €14,000 (Nurmi *et al.* 2003), and that there are over 7,000 patients per year suffering from hip fracture (Kannus *et al.* 2006). Even higher costs and numbers of hip fractures have been reported in other countries (van Balen *et al.* 2001, Braithwaite *et al.* 2003, Zethraeus *et al.* 1997). To prevent increases in hip fracture incidence and costs, fracture-preventative and fracture-predictive studies investigating the mechanism of fractures are needed.

Falls are a major cause of hip fracture and frequently associated with osteoporosis. An osteoporotic fracture is typically related to reduced bone strength and falling. Among individuals aged over 65 years, falling is the primary factor in over 90% of hip fractures, and a history of falls is involved in an increased risk of hip fractures (Cummings & Klineberg 1994, Cummings *et al.* 1995).

Dual-energy X-ray absorptiometry (DXA) is the standard diagnostic tool in the assessment of hip fracture risk. However, it has been shown that the predictive value of DXA-based bone mineral density (BMD) to evaluate individual fracture risk is inadequate (Kanis 2002, Stone *et al.* 2003), and that it is insufficient to accurately predict who will and who will not encounter a fracture (Marshall *et al.* 1996, Schuit *et al.* 2004). Recently, FRAX™ was developed as a tool to assess the 10-year probability of fracture (Kanis *et al.* 2008). It is based on a set of clinical risk factors with or without BMD. Still, DXA-based methods do not result in optimal estimation of individual fracture risk.

In addition to BMD, the structure and geometry of a femur are important factors in the estimation of hip fracture risk (Bergot *et al.* 2002, Pulkkinen *et al.* 2004, Pulkkinen *et al.* 2008). Using appropriate method for image analysis in the estimation of hip fracture risk, structural parameters of trabecular bone and bone geometry have been shown to predict *in vitro* femoral fracture loads with similar accuracy as DXA (Pulkkinen *et al.* 2008). It has also been suggested that bone geometry influences proximal femoral stress distribution under given loading conditions (Voo *et al.* 2004), and that risk factors for cervical and trochanteric hip fractures differ (Gnudi *et al.* 2002, Mautalen *et al.* 1996, Pulkkinen *et al.* 2011). In addition, femoral neck fractures seem to have lower fracture loads under similar loading conditions compared to trochanteric ones (Pulkkinen *et al.* 2006).

The assessment of fracture type may thus improve the estimation of hip fracture risk.

Computational finite element (FE) analysis is an effective method for studying the biomechanical characteristics of a hip fracture. FE analysis has been recognized as a noninvasive tool to estimate femoral fracture load and hip fracture type (Lotz *et al.* 1991a, Lotz *et al.* 1991b, Keyak *et al.* 1998, Keyak *et al.* 2001). However, a compromise between computational (*i.e.,* generation and solution) time and accuracy of a FE model typically has to be made in order to achieve more effective solutions for clinical use. Complex FE models and their analysis require high computational power and time. Therefore, more straightforward models with less time-consuming generation and analysis have to be developed. However, accurate models are required as a reference for reduced simulation approaches.

In this study, CT-based FE models were developed to estimate experimental femoral fracture load and hip fracture type in a sideways fall loading configuration (Eckstein *et al.* 2004). A simplified simulation model was generated to assess the impact of proximal femur geometry on the hip fracture type. A subject-specific FE model was developed to estimate femoral fracture load. From this model, a reduced representation was created in order to evaluate the predictive value of a more simplified model, based solely on cortical bone, in the estimation of experimental femoral fracture load. The predictive value was compared with that of DXA, and with that of the subject-specific FE model.

2 Review of the literature

2.1 Structure and physiology of bone

The main functions of bone involve supporting the body, enabling mobility, protecting organs, storing fat and minerals, and forming blood cells. Bone structure is a composite of 70% mineral, 22% organic matrix, and 8% water (Reis *et al.* 2011). The organic bone matrix is largely type I collagen and the substance of inorganic bone matrix is mainly calcium phosphate in the form of hydroxyapatite crystals. This kind of composition results in stiff but tough material, and the skeleton's ability to maintain the shape of the body results from the rigidity and hardness of bone. (Jee 2001.) In general, mineral contributes to the hardness, organic matrix to the elasticity, and water to the viscoelasticity of bone.

Bones can be classified according to their shape into long (e.g. femur and humerus), flat (e.g. parietal bones), short (e.g. carpal bones), and irregular (e.g. vertebra) bones. Long bones are designed to carry compressive loads and resist bending, short bones to resist mainly compressive loads, and flat bones to protect organs or to provide a base for the origin of muscles. A long bone comprises a cylindrical shaft (diaphysis) and two wider and rounded ends (epiphyses) (Fig. 1). The metaphysis connects the diaphysis with the epiphysis. The long bones are mostly made of cortical or compact bone and the short bones of trabecular or cancellous bone. In adult human skeletons, approximately 80% of total skeletal mass is cortical bone and the remaining 20% trabecular bone. Dense cortical bone forms the outer layer of all bones and spongious trabecular bone can be found in the inner parts of bones, but the distribution of cortical and trabecular bone varies considerably between individual bones. The diaphysis consists mainly of cortical bone, which surrounds the medullary cavity. (Currey 2002, Jee 2001.)

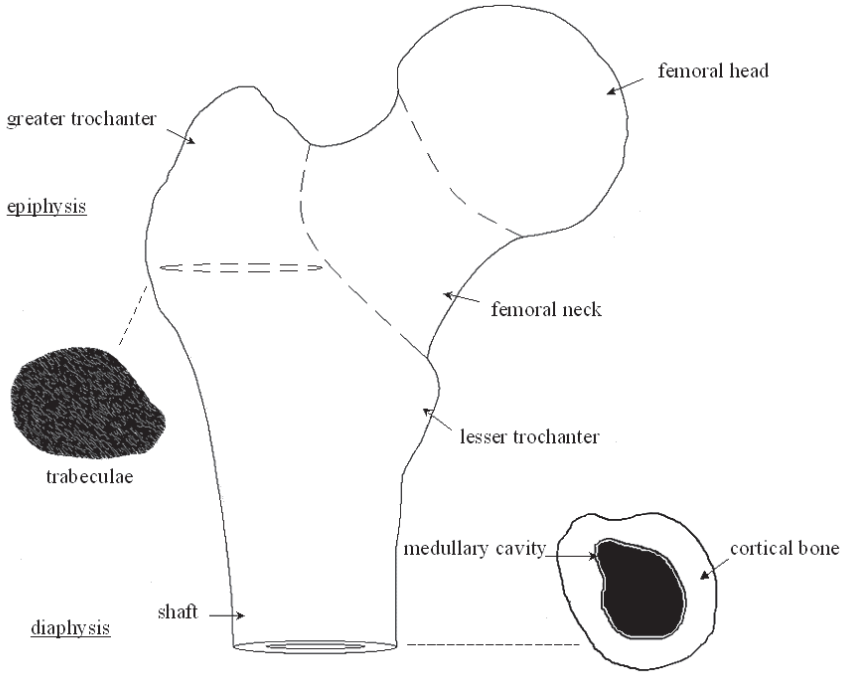

Fig. 1. Structure of a typical long bone (proximal femur).

There are two main types of cortical or trabecular bone, woven and lamellar. In fracture healing, new bone is formed in woven type, and it is replaced by lamellar bone (Jee 2001). The basic structural unit of cortical bone is the osteon or Haversian system, wherein the Haversian canal contains blood vessels and nerves, which are surrounded by lamellae (Enoka 2002). The lamellae consist of collagen fibers, which have different orientations in adjacent lamellae (Rho *et al.* 1998). The collagen fibers are composed of many collagen fibrils, which are composed of collagen molecules and related bone crystals (Enoka 2002). In trabecular bone the structural unit is the hemiosteon or trabecular packet that is ideally shaped like a shallow crescent (Jee 2001).

2.1.1 Bone modeling and remodeling

The osteoclasts and osteoblasts are cells that resorb and form bone, respectively. Resting osteoblasts are called bone-lining cells. The osteoblasts can also differentiate into osteocytes that are left behind and embedded as the bone formation goes on. These cells are involved in bone modeling and remodeling. (Jee 2001.) Modeling largely takes place in different bone surfaces continuously during growth, while remodeling is a process that occurs cyclically throughout life span. After activation, the modeling process continues with either formation or resorption drift, whereas the remodeling cycle always progresses from resorption to formation. (Parfitt 2009.) During modeling, bone is formed faster on the outer surface (periosteum) than it is resorbed on the inner surface (endosteum) of a bone. Modeling allows the modification of bone architecture and mass when mechanical conditions change during growth. Remodeling takes care of producing and maintaining biomechanically and metabolically competent bone. The bone turnover or periodic replacement of bone helps to maintain load bearing and to repair structural damage. The functional group of cells that conducts removal and replacement of bone is called basic multicellular unit (BMU) or bone remodeling unit (BRU). (Jee 2001.)

2.1.2 Mechanical properties of bone

At structural level, load-deformation relation (Fig. 2) can be determined from mechanical testing of a bone. The linear part of the curve represents the elastic deformation, and the slope of the elastic region the stiffness or rigidity of the structure. After a yield point, bone starts to yield nonlinearly, and goes through irreversible plastic deformation. The ultimate load (force at failure) is the load (N) where bone breaks. The area under the load-deformation curve measures the work needed to cause a failure. (Turner & Burr 2001.)

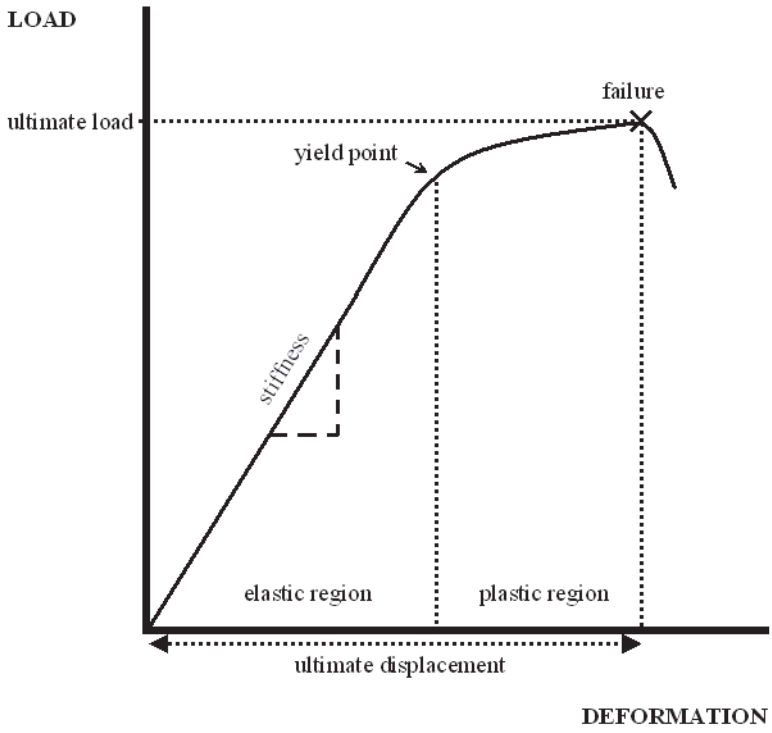

Fig. 2. Characteristic load-deformation curve from mechanical testing of a bone. See text for explanations.

Normalized load and normalized deformation are described as stress (force per unit area) and strain (relative change in length), respectively. The measures represent the intrinsic material properties of bone, which can be determined for tensile, compressive, shear, and bending loads. At tissue level, bone material properties are commonly characterized by stress-strain curve (normalized load-deformation relation). A load is applied to a bone specimen and the resulting deformation is measured. Normal stresses occur when tensile loads elongate the specimen or compressive loads shorten and widen the specimen. The material properties of bone can be characterized by measuring the slope of the elastic region called Young's modulus or elastic modulus, and the stress and strain values (Table 1) in yielding and in failure. (Enoka 2002.)

Table 1. Basic parameters of bone mechanical properties.

Parameter	Equation	Unit	Description
Stress	$\sigma = \frac{F}{A}$	[Pa] or [N/m^2]	F is the applied force and A the cross-sectional area
Strain	$\varepsilon = \frac{\Delta l}{l}$	% or με	Δl is the change in length and l the original length
Young's modulus	$E = \frac{\sigma}{\varepsilon}$	[Pa] or [N/m^2]	σ is the stress and ε the strain in the elastic region

As a composite material, bone typically has a higher fracture load in compression than in tension. Material properties such as elastic modulus and yield stress are commonly higher in cortical than in trabecular bone as seen in Table 2, in which these material properties are represented measured with different techniques for a typical long bone (femur).

Table 2. Elastic modulus and yield stress of the femur measured in different studies.

Reference	Method	Anatomic site	Bone specimen	E [GPa]	σ_{yt} [MPa]	σ_{yc} [MPa]
Bayraktar *et al.* 2004	Experimental and FEA	Neck	Trabecular	18.0 ± 2.8 (N = 12)	84.9 ± 11.2 (N =6)	135.3 ± 34.3 (N = 6)
		Mid-diaphysis	Cortical	19.9 ± 1.8* (N = 74)	107.9 ± 12.3 (N = 74)	N/A
Kaneko *et al.* 2003	Experimental	Diaphysis	Trabecular	22.7 ± 1.7* (N = 16) 23.0 ± 1.8** (N = 16)	83.9 ± 8.8 (N = 7)	153.0 ± 16.5 (N = 7)
Turner *et al.* 1999	Nanoindentation	Distal femur	Trabecular	18.1 ± 1.7 (N = 30)	N/A	N/A
		Mid-diaphysis	Cortical	20.0 ± 0.3 (N = 60)	N/A	N/A
Zysset *et al.* 1999	Nanoindentation	Neck	Trabecular	11.4 ± 5.6 (N = 8)	N/A	N/A
			Cortical	15.8 ± 5.3 (N = 8)	N/A	N/A
		Mid-diaphysis	Cortical	19.1 ± 5.4 (N = 8)	N/A	N/A

E Young's modulus, * in tension, ** in compression, σ_{yt} yield stress in tension, σ_{yc} yield stress in compression, N number of samples, N/A not applicable, values given as mean ± SD.

2.1.3 Structural properties of bone

Bone geometry largely defines its structural properties. The femur of an adult can carry more load than the femur of a child, mainly because of the difference in bone cross-sectional area (CSA) or size. (Enoka 2002.) In other words, if bone is under large stresses, it must have large cross-sectional area to withstand the stresses. Loads determine bone structure, and vice versa. Bone tends to adapt its geometry to the surrounding mechanical conditions. (Seeman & Delmas 2006.) For example in the proximal femur, the shape of the femoral neck is more elliptical at the neck-shaft junction where bending stresses are greater, whereas the shape is more circular near the femoral head where compressive stresses are greater (Zebaze *et al.* 2005). In addition to bone size and shape, bone microarchitecture, which refers to the cortical porosity and the characteristics of trabeculae (amount, orientation, thickness, connectivity), also plays a role when defining bone mechanical competence (Dempster 2003).

2.1.4 Bone adaptation to mechanical usage as a system

It is stated in Wolff's law (Wolff 1892) that mechanical loadings can make bone's architecture change (Frost 1994). Externally applied forces largely influence the growth and ossification of the skeleton (Jee 2001). Frost (Frost 1987) suggested that the mechanism monitoring the fit of bone mass to mechanical usage and controlling longitudinal growth, modeling, and BMU-based remodeling activities could be referred to as a mechanostat. This hypothesis is based on the idea that there is a minimum effective strain (MES) threshold, and strains above this threshold (overload) evoke a response that leads to increase in the bone mass, while strains below the threshold (underload) trigger a response that causes bone loss (Jee 2001). Modeling and remodeling operate within different strain ranges, which means that when modeling is active on a bone surface, remodeling is inactive, and vice versa (Frost 1997). Strains above 1,500 microstrain trigger the modeling-dependent bone gain while strains below 200 microstrain evoke the remodeling process (Jee 2001). These explanations help us to understand how bone response to mechanical usage works.

2.1.5 Age-related bone loss

Human bone mass increases during growth, starts to level off in young adults, and finally begins to decrease after about 30 years (Wasnich 1997). There are many factors influencing age-related bone loss, tendency to fall, and fracture risk, for example decrease in estrogen (Lindsay 1994, Schiessl *et al.* 1998), decrease in calcium and vitamin D (Peacock 1998, Lau & Baylink 1999), and physical inactivity (Marcus 1989, Coupland *et al.* 1993). Estrogen deficiency is a major cause of bone loss in the first two decades after menopause (Richelson *et al.* 1984). Decrease in bone density with aging is also partly explained by increased parathyroid hormone secretion resulting from vitamin D deficiency and low calcium intake (Jee 2001). Decreased vitamin D and calcium levels have very similar effects on the skeleton, because vitamin D ($1,25(OH)_2$ vitamin D) is a major regulator for calcium homeostasis and skeletal metabolism. Vitamin D and calcium insufficiencies can be prevented with sunlight exposure and calcium-rich foods, respectively, and with dietary supplements. Nevertheless, unnecessary vitamin D intake should be avoided as it may also lead to osteoporosis. (Peacock 1998.) Active lifestyle and exercise maximize peak bone mass, reduce age-related bone loss, maintain muscle power, body balance and walking ability, and prevent falls. Therefore, it is recommended to stay active throughout life in order to maintain bone health. (Iwamoto *et al.* 2008.)

Loss of bone during life is the main cause of osteoporosis, a bone disease characterized by a decrease in bone mass and a decline in bone microarchitecture and bone strength, which leads to increased bone fragility and eventually to an increased risk of fracture (Jee 2001). Osteoporosis advances when bone resorption exceeds bone formation, and therefore it is not only a disease of the elderly as is often thought. However, osteoporosis will increase with an increase of life expectancy (Jee 2001), so it is a governing condition of the elderly (Rizzoli *et al.* 2009). Approximately three to four out of ten women over the age of 50, and one in eight men, will suffer fracture related to osteoporosis in their lifetime (Jee 2001).

Osteoporosis is functionally defined on the basis of bone mineral density assessment or bone mineral content (BMC) assessment. The World Health Organization (WHO) suggests defining osteoporosis on the BMD T-score, which is standard deviation (SD) from the mean for young adult Caucasian women. T-score below -2.5 indicates osteoporosis, while T-score between -1.0 and -2.5 refers to osteopenia or low bone mass, which is a preliminary stage of

osteoporosis. If T-score is below -2.5 and fracture is present, the condition is called severe osteoporosis. T-score over -1.0 indicates normal bone mass. (WHO 1994, Kanis & the WHO Study Group 1994, Kanis *et al.* 1994.) While a T-score represents how much a patient's bone mass deviates from the mean bone mass of a healthy adult, a Z-score compares bone density to the mean for people of same age and gender. The use of Z-score to imply osteoporosis is somewhat doubtful, because it assumes that the predominance of osteoporosis does not increase with age. (Kanis *et al.* 2000.) However, the use of Z-score is advisable for the diagnosis of osteoporosis in premenopausal women and in children (Leib *et al.* 2004).

FRAX™ is a fracture risk assessment tool developed by WHO (Kanis *et al.* 2008). It is based on the use of clinical risk factors alone or with BMD. The clinical risk factors evaluated in FRAX™ consist of body mass index (BMI), history of fracture, a parental history of hip fracture, use of oral glucocorticoids, rheumatoid arthritis and other secondary causes of osteoporosis, current smoking, and alcohol intake of 3 or more units daily. As a result, the analysis gives the 10-year probability of hip fracture.

2.2 Hip fracture

Fractures associated with osteoporosis or osteoporotic fractures comprise fractures such as those of the spine, humerus, forearm, pelvis and hip (Kanis *et al.* 2001). These fractures are a common cause of disability and cause major medical care costs (Cummings & Melton 2002). Proximal femoral fracture or hip fracture is considered to be the most serious result of osteoporosis among the elderly (Cummings & Melton 2002), yet osteoporotic fractures at other sites are much more common in younger individuals (Johnell & Kanis 2006). Bone weakens and neuromuscular function declines with advancing age, increasing the risk of fractures. The clinical and public health importance of osteoporosis is due to these fractures. (Cummings & Melton 2002.) Nevertheless, the increasing occurrence of fractures with age is not evidence of osteoporosis, since a rising incidence of falls could also be a cause of fracture (Kanis *et al.* 2001). In any case, an osteoporotic hip fracture is usually related to both reduced bone strength and falling. Still, hip fractures are strongly fall-related (Dargent-Molina *et al.* 1996, Willig *et al.* 2003).

Hip fractures may occur spontaneously (Parker & Twemlow 1997) or after a sideways fall onto the greater trochanter (Hayes et al. 1996). Spontaneous hip fractures typically occur suddenly in the proximal femur, causing severe pain, and

eventually falling. (Parker & Twemlow 1997.) In a sideways fall, a trochanteric fracture typically occurs with high fracture load levels, while a cervical fracture is more common in femurs with lower bone strength (Pulkkinen *et al.* 2006). During normal gait, maximum compressive stresses occur in the inferior and tensile stresses in the superior femoral neck. The stress state is reversed in the neck during a fall to the side, and maximum compressive stresses occur in the superior and tensile stresses in the inferior femoral neck. (de Bakker *et al.* 2009, Lotz *et al.* 1995.) The body weight and falling height of the body affect directly the impact force. The effects of the impact vary depending on the level of soft tissue and clothing padding on the greater trochanter. (Majumder *et al.* 2008.)

2.2.1 Hip fracture types

Hip fractures can be categorized into two main groups, trochanteric and cervical (femoral neck) fractures, according to the fracture location at the proximal femur (Fig. 3). These trochanteric and cervical main groups are typically divided into subgroups (Müller & Nazarian 1981), which consist of pertrochanteric and intertrochanteric fractures, and subcapital and transcervical fractures, respectively.

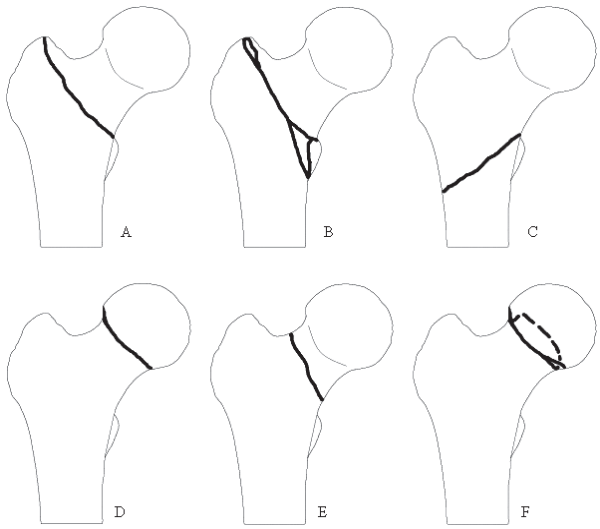

Fig. 3. Typical trochanteric and cervical hip fractures. (A) Simple pertrochanteric fracture, (B) multifragmentary pertrochanteric fracture, (C) intertrochanteric fracture, (D) subcapital fracture, (E) transcervical fracture, and (F) displaced subcapital fracture.

Healing and treatment of cervical and trochanteric hip fractures differ. Healing of cervical fractures may be hindered by sensitive blood supply to the femoral head. This is not a problem in trochanteric fracture cases, yet there may be substantial blood loss in the area. Cervical fractures may be treated by fixing the fracture and protecting the femoral head and trochanteric fractures by prolonged traction. However, a hip fracture is often treated by surgery. (Parker & Johansen 2006.)

Several studies have stated that the predictive factors for the cervical and trochanteric fracture types differ (Duboeuf *et al.* 1997, Partanen *et al.* 2001, Schott *et al.* 1998). This is also observed in more recent studies, which suggest that trochanteric fractures are mainly determined by BMD (Pulkkinen *et al.* 2004, Schott *et al.* 2005), while cervical fractures are primarily defined by bone geometry (Gnudi *et al.* 2002, Pulkkinen *et al.* 2010). Overall, all these investigations support the statement that the hip fracture types should be studied separately (Mautalen *et al.* 1996).

2.2.2 Imaging methods for evaluating hip fracture risk

Common methods for measuring BMD, one of many contributors to hip fracture risk (Cefalu 2004), are DXA and quantitative computed tomography (QCT). The DXA device uses two X-ray beams of different energy levels to determine areal BMD. With a QCT scan, a real volumetric BMD can be measured using a hydroxyapatite phantom, composed of two density phases representing the water-like and bone-like parts for density calibration. BMD of cortical and trabecular bone compartments can also be analyzed separately with QCT. (Ito 2011.) QCT has been suggested to estimate fracture load variance for cervical fracture better than DXA-provided BMD (Bousson *et al.* 2006). However, costs and X-ray radiation exposures are higher in CT than in DXA. A CT scanner produces image slices of the body in the axial plane, and the final image is generated from this series of images. Peripheral QCT (pQCT), micro-CT (μCT) and synchrotron CT (SR-CT) devices are used to scan a peripheral part of the body, bone microstructure, and the micro- to nanostructure of bone, respectively (Ito 2011).

The Singh index is a method based on radiography and trabecular pattern of the upper femur that can be used for the assessment of osteoporosis index (Singh *et al.* 1970). For the diagnosis and grading of osteoporosis, and thus, for somewhat rough fracture risk estimation, the structure of trabeculae was evaluated, and six different trabecular patterns with increasing bone loss were found (Singh *et al.* 1970). Later, plain radiographs have been used for the

evaluation of bone geometry (Casper *et al.* 2012, Gregory *et al.* 2004) and trabecular bone structure (Benhamou *et al.* 2001, Huber *et al.* 2009, Vokes *et al.* 2006). The combination of proximal femoral trabecular bone structure and geometry has been suggested to improve the prediction of hip fracture (Chappard *et al.* 2010, Karlsson *et al.* 1996, Pulkkinen *et al.* 2008).

An alternative for these radiative methods are ultrasound (US) based procedures (Barkmann *et al.* 2010, Hans & Krieg 2008, Schott *et al.* 1995). Ultrasounds are high frequency sound waves that bounce back from the internal organs. Piezoelectric material generates and receives the sound waves, which are then displayed as a real-time image. (Angelsen 2000.) Ultrasound has been suggested to be better correlated to fracture type than DXA, to discriminate subjects with hip fracture to the same degree as DXA, and to provide a signal of fracture risk independent of BMD (Schott *et al.* 1995). Heel quantitative ultrasound device has also been shown to be predictive of hip fracture risk (Krieg *et al.* 2006, Stewart *et al.* 2006).

Magnetic resonance imaging (MRI) is a reliable method for diagnosing hip fracture and a valuable non-ionizing radiation method to evaluate hip fracture risk (Zuckerman 1996). Compared with traditional radiography and DXA, CT and MRI, which are three-dimensional imaging methods, provide information on structural properties more effectively. CT scanners are easier to operate than MRI devices and the availability of CT equipment is better, but CT scans produce high radiation doses. (Genant *et al.* 2008, Ito 2011.) Nevertheless, MRI allows three-dimensional imaging of trabecular bone (Donnelly 2011) and can therefore detect for example age-related changes in trabecular structure (Majumdar *et al.* 1997).

2.2.3 Experimental mechanical testing of the femur

Mechanical testing of a cadaver femur is typically performed in a vertical (axial) loading configuration (Dalén *et al.* 1976) or in a side impact (lateral or sideways fall) loading configuration (Bouxsein *et al.* 1995, Courtney *et al.* 1994) (Fig. 4). The shaft of the proximal femur is installed in a loading device by embedding it into plastic resin or by clamping it in place (Turner & Burr 2001). Force is applied to the femoral head (Courtney *et al.* 1994) or to the greater trochanter (de Bakker *et al.* 2009, Eckstein *et al.* 2004) until the femur fractures.

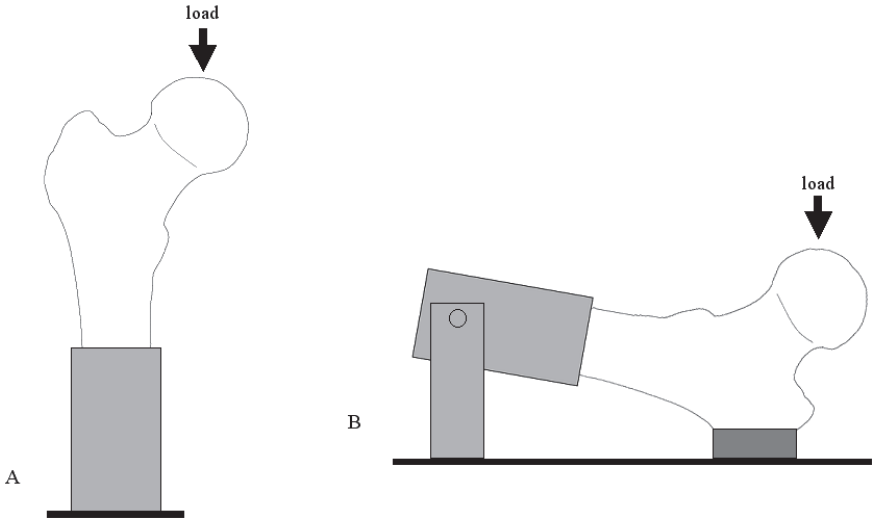

Fig. 4. Typical experimental mechanical testing of a proximal femur in the (A) axial and (B) sideways loading configuration.

In experimental mechanical testing fracture load is typically defined as the peak value of the load-deformation curve. Fracture loads measured in previous studies using a similar sideways fall configuration (*i.e.*, the femoral shaft positioned 10 degrees from the horizontal and the femoral neck 15 degrees from the vertical in internal rotation) are represented in Table 3. The sideways fall configuration simulates the biomechanics of the hip fracture under realistic conditions and patterns (Lochmüller *et al.* 2002, Turner & Burr 2001).

Table 3. Experimental femoral fracture loads from experimental studies simulating a fall on the greater trochanter.

Reference	N (F/M)	Age range (mean)	Fracture load [N]
Bouxsein *et al.* 1995	16 (6/10)	59–96 (76)	3680 ± 1540
Courtney *et al.* 1995	8 (4/4)	59–83 (74)	3440 ± 1330
de Bakker *et al.* 2009	12 (6/6)	72–93 (84)	4032 ± 370
Eckstein *et al.* 2004	108 (30/24)	52–100 (79)	3900 ± 1652* 3951 ± 1659**

F female, M male, N number of samples, * for 54 left femurs, ** for 54 right femurs, fracture load given as mean ± SD.

2.3 Finite element method

Finite element analysis is a useful method for simulating the mechanical behavior of a structure. With FE analysis, a complex structure can be divided into geometrically more simple finite components or elements that are attached to each other by connection points called nodes. The elements connected via nodes form an element mesh. Material properties of the structure are implemented to the element mesh. Loading and boundary conditions for the structure are applied to complete a FE model.

Generally, mechanical FE analysis is based on the equilibrium equation

$$KU = F\,, \tag{1}$$

where K is the global stiffness matrix, U is the global nodal displacement, and F is the global nodal force. The global stiffness matrix depends on material and geometrical properties of the element mesh, and it is composed of the stiffness matrices of individual elements. The boundary conditions are applied to the U and F. The equilibrium equation is solved to find the unknown nodal displacements.

Two main methods for determining material yielding used in biomechanical FE modeling are the von Mises (von Mises 1913) and Drucker-Prager (Drucker & Prager 1952) criteria. The von Mises yield theory for ductile materials in static loading states that the material will yield when the von Mises stress exceeds the yield strength of the material (Logan 2007). In terms of the three principal stresses (σ_1, σ_2, σ_3), the von Mises stress can be expressed as

$$\sigma_{VM} = \sqrt{\frac{(\sigma_1 - \sigma_2)^2 + (\sigma_2 - \sigma_3)^2 + (\sigma_3 - \sigma_1)^2}{2}}\,. \tag{2}$$

The Drucker-Prager yield criterion is a modification of von Mises yield criterion and is often applied to composite materials. The Drucker-Prager yield strength can be described in terms of mean stress (σ_m) and von Mises stress as

$$k = 3\alpha\sigma_m + \sigma_{VM}\,, \tag{3}$$

in which α is a material constant.

2.3.1 Finite element analysis

FE software tools are used to analyze complex problems. Analyzing a FE model requires knowledge of the simulated system and pre-processing actions from the

operator, before calculations can be executed by the FE solver. The actions performed by the operator and the solver are described in Fig. 5.

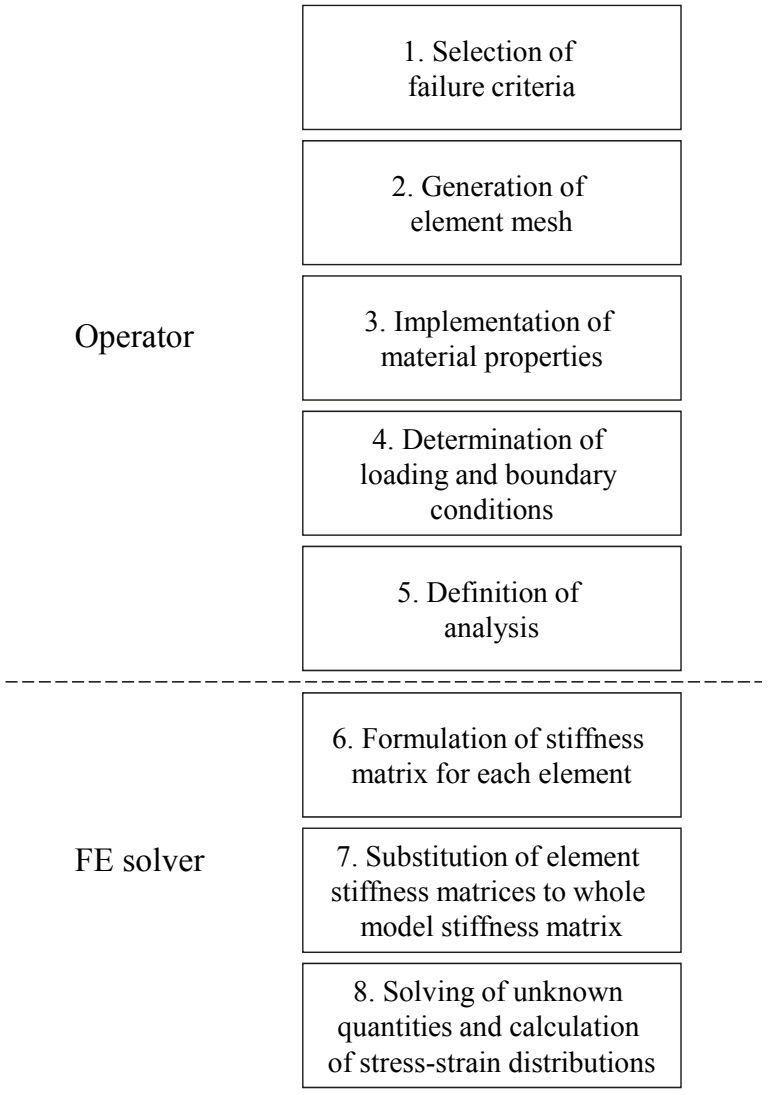

Fig. 5. Typical actions performed by the operator and the computational solver when analyzing a simulation model in software for finite element method.

2.3.2 Finite element modeling of hip fracture

As described above, complex mechanical systems can be solved effectively using FE analysis. This has also been noticed in the field of biomechanics wherein FE analysis has been recognized as a noninvasive tool to estimate hip fracture risk.

Selection of failure criteria

Strain-based criteria perform well in a sideways fall configuration when evaluating experimental femoral fracture load using FE analysis (Keyak & Rossi 2000). In addition to strain criterion, Von Mises yield criterion and Drucker-Prager yield criterion are commonly used in hip fracture FE studies. Drucker-Prager criterion has been suggested to be more suitable for brittle materials such as bone (Bessho *et al.* 2007), in which tensile strength is smaller than compressive strength (Cordey & Gautier 1999). Nevertheless, the von Mises yield criterion forms the basis of the Drucker-Prager yield criterion, wherein mean stress is also included to represent pressure-sensitivity.

After yielding, a failure of an element is typically determined to occur when FE stress or strain exceeds the set stress or strain limit. The stress and strain limits can be obtained from experimental data or from a training set of FE models based on experimental mechanical testing. The selected yield and failure criteria can then be integrated into material properties and FE analysis.

Generation of element mesh

In order to generate a FE model of a proximal femur, the bone first has to be segmented from radiological image and then meshed into an understandable format for the FE software. Segmentation can be done manually or semi-automatically with segmentation software using grey scale value related to material distribution and outer contour definition to separate bone from its surroundings.

After segmentation, the femur is an individual object in the segmentation software, and it can be exported to FE software as an element mesh representing the geometry of the actual bone (Fig. 6). The three-dimensional solid element type of the mesh can be either tetrahedral or hexahedral. In addition, the proximal femur can be separated into cortical and trabecular bone compartments in a segmentation software using grey-value thresholds and inner contour for the

cortical bone. Before exporting the mesh to FE software, some material properties (e.g. Young's modulus) can also be implemented to the segmented femur or separately to the different bone compartments using the grey-value information of the bone.

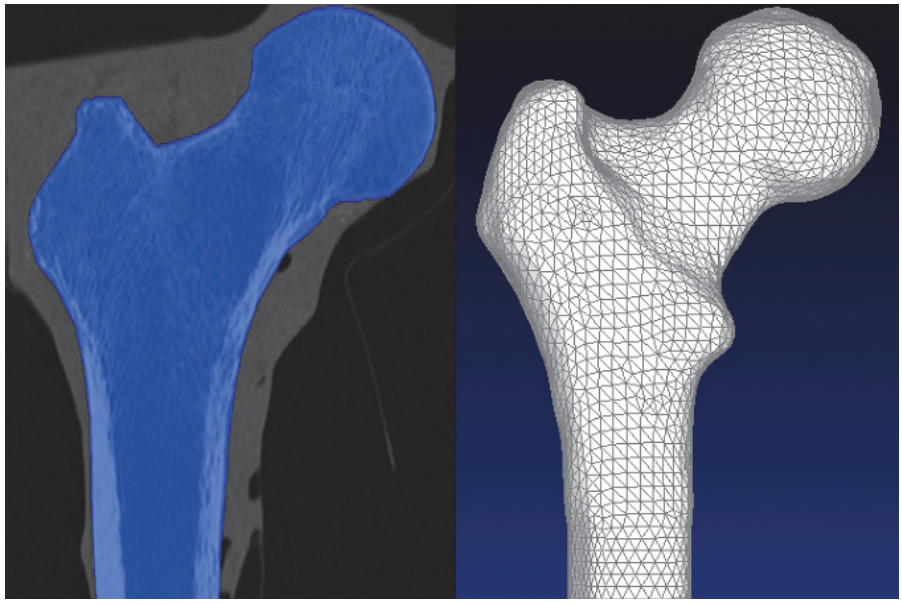

Fig. 6. Segmentation of a proximal femur from CT scans.

Implementation of material properties

Bone is identified as an orthotropic material, but generating and analyzing a bone FE model with orthotropic material properties requires more time and computational power than a model with isotropic material properties. Moreover, the differences between these material property assignments are small (Peng *et al.* 2006). Therefore, for example proximal femur is largely modeled with isotropic material.

For a three-dimensional FE model, the material properties of a proximal femur are derived from a volumetric CT image. Each element contains its own grey-value information and heterogeneous material properties can thus be implemented to the mesh. The Young's modulus and the yield stress can be derived from the ash density, which represents stiffness and strength of bone

tissue and is strongly correlated to QCT density, and which can be used with nearly equal precision (Keyak *et al.* 1994). This relation links the physical measures of bone density and mechanical properties to QCT data.

Determination of boundary conditions

Boundary conditions are implemented to a FE model to simulate real-life or experimental situations. These conditions are properties that are externally positioned to a system. The properties can be applied to the nodes and elements of the FE model to simulate the behavior of the system in space. For example, when simulating a proximal femur in a sideways loading condition, a vertical load can be distributed to the nodes on the femoral head, and the nodes on the surface of the greater trochanter can then be fixed in the loading direction, and displacements of the nodes at the distal end of the femoral shaft largely restricted (Verhulp *et al.* 2008). The load can alternatively be applied on the greater trochanter depending on the experimental setup.

Analysis of FE model

Based on the user-defined properties and conditions, the FE solver finds a solution to the corresponding problem. It first formulates a stiffness matrix for each element, and then substitutes the element stiffness matrices to the whole model stiffness matrix. After that, it solves the unknown quantities, and finally calculates the stress-strain distributions.

3 Purpose of the study

This study examines hip fracture by using the finite element approach. Simulation was done for CT-based FE models in the estimation of experimentally measured fracture type and fracture load of the proximal femur in a sideways fall loading configuration. The specific aims of this study were:

1. To test the hypothesis that individual proximal femur geometry results in strain distributions that coincide with the occurrence of cervical versus trochanteric hip fracture patterns.
2. To assess the accuracy of a bilinear elastoplastic FE in the estimation of the experimentally measured fracture load.
3. To assess the predictive value of a FE model including only cortical bone in the estimation of the experimentally measured fracture load.

4 Materials and Methods

4.1 Subjects

Cadaver femurs from a larger experimental study (Eckstein *et al.* 2004) were obtained from the Institute of Anatomy at the Ludwig Maximilians University of Munich (Germany) (Table 4). Based on biopsies of the femurs, individuals with bone diseases other than osteoporosis or osteopenia were excluded.

Table 4. Summary of study samples.

Study	Samples F/M	Age (years)
I	26/0	83 ± 9
II, III	41/20	80 ± 9

F female, M male, age is given as mean ± SD.

4.2 Imaging methods

The femurs were scanned using a multi-detector CT (MD-CT) scanner and DXA. CT images were used for generating the FE model, and DXA was used as a reference method.

4.2.1 Computed tomography scans (I-III)

Femurs were scanned with a 16-row MD-CT scanner (Sensation 16; Siemens Medical Solutions, Erlangen, Germany). The femurs were degassed, packed in airproof plastic bags filled within a formalin/water solution, and placed in the MD-CT scanner in a position that was comparable to that used in the *in vivo* exam of pelvis and proximal femur. The slice thickness was 0.75 mm. The settings were 120 kVp and 100 mAs, a 512 x 512 pixels image matrix, a field of view of 100 mm, and the in-plane spatial resolution was approximately 0.25 mm x 0.25 mm using a high spatial resolution reconstruction algorithm (kernel U70u). All specimens were scanned on a reference phantom (Osteo Phantom, Siemens, Erlangen, Germany), which consisted of two density phases, a 0 mg hydroxyapatite/cm^3 and a 200 mg hydroxyapatite/cm^3 phase representing the water-like and bone-like parts of the phantom, respectively.

4.2.2 Dual-energy X-ray absorptiometry (I, III)

In vitro DXA scans of the femurs were obtained using a standard narrow fan beam scanner (GE Lunar Prodigy, GE Lunar Corp., Madison, WI, USA) with the femoral specimens submerged in a water bath. Standard positioning was used across all specimens, and the proximal femoral BMD and BMC values were evaluated with the software provided by the manufacturer. Femoral neck, trochanteric and total values were assessed.

4.3 Mechanical testing (I-III)

After the CT and DXA scans, the cadaver femurs were mechanically tested for failure, simulating a fall on the greater trochanter (Eckstein *et al.* 2004). The femoral shaft was positioned at 10º from horizontal, the neck was positioned at a 15º internal rotation, and the femoral head faced downward. The length of the femoral shaft above the fixation on the shaft was four times the head diameter. The femoral head was fitted into a half of a tennis ball inside the other half of the tennis ball. The loads were applied at a rate of 6.6 mm/s to the greater trochanter through a pad, using a material testing machine (Zwick 1445, Ulm, Germany). The fracture load (maximal load encountered during the test) was determined from the load-deformation curve. The fracture patterns were classified from the broken bones to cervical and trochanteric according to the standard AO classification. Subcapital and transcervical fractures were classified to cervical fractures and pertrochanteric, intertrochanteric, and subtrochanteric fractures to trochanteric fractures.

4.4 Finite element models

For study I, the proximal femurs were manually segmented with MD-CT datasets and MeVisLab (version 1.6, MeVis Research GmbH, Bremen, Germany). The two-dimensional slices of the proximal femur were segmented to cortical and trabecular bone and converted to three-dimensional surfaces. Femap (version 9.2.0, UGS Corp., Plano, TX, USA) with NX Nastran (version 4, UGS Corp., Plano, TX, USA; MSC Software Corporation, Santa Ana, CA, USA) was used for pre-processing, analyzing, and post-processing the FE models. The minimum cortical thickness of the proximal femur was adjusted to 1 mm using a script made in Matlab (R2006b, MathWorks, Inc., Natick, MA, USA).

For studies II and III, the proximal femurs were semi-automatically segmented with MD-CT datasets and Mimics (v12.1, Materialise, Leuven, Belgium). Trabecular and cortical bone was modeled individually. Femap (Femap, version 10.1., UGS Corp., Plano, TX, USA) software was used for the pre-processing, and MD Patran (2008 r1, MSC.Software Corporation, Santa Ana, USA) software was used for the post-processing of the models. MD Nastran (R3, MSC.Software Corporation, Santa Ana, USA) was used for the calculation. In study III, elements of the trabecular bone of the full FE model were removed and only cortical bone was simulated. Similar element size, cortical thickness, loading configuration, material properties, yield criterion and FE analysis for cortical bone model were used as in full FE model.

Trabecular and cortical bone were modeled with tetrahedral elements with element size of 3 mm and a minimum cortical thickness of 1 mm. A material close to that of a tennis ball was used in the FE simulated pad and tennis ball. A homogenous isotropic material was used in the simulated cortical bones, and a Poisson's ratio of 0.33 was used in the simulated bones (Lengsfeld *et al.* 1998).

In study I, a homogenous Young's modulus of 1.1 GPa for the trabecular bone and 15 GPa for the cortical bone was used (Lengsfeld *et al.* 1998). In studies I and II, the subject-specific maximum density value of the cortical bone was used to obtain the isotropic Young's modulus for the simulated cortical bone. For material heterogeneity (study II), an average gray value of all of the voxels inside an element was calculated in Mimics. The bone equivalent density (ash density, ρ_{ash}) was then defined by assuming a linear relationship in which the density is proportional to the attenuation. Trabecular bone was considered to be a heterogeneous isotropic material, and the subject-specific material properties were assigned to each trabecular bone element. Applied mechanical properties of studies II and III are summarized in Table 5.

Table 5. Summary of the applied mechanical properties for FE model estimating the femoral fracture load.

Study	Parameter	Calculus	Reference
II, III	Young's modulus	$E = 10.095\rho \frac{MPa}{mg/cm^3}$	Duchemin *et al.* 2008
II, III	Yield stress	$\sigma_{yc} = 114 \frac{\rho_{ash}}{g/cm^3}^{1.72} MPa$	Keller 1994
II		$\sigma_{yt} = 137 \frac{\rho_{ash}}{g/cm^3}^{1.88} MPa$	Keyak *et al.* 1994
II, III	Post-yield modulus	5% of E (MPa)	Bayraktar *et al.* 2004

ρ, equivalent CT density (mg/cm^3); ρ_{ash}, ash density (g/cm^3); σ_{yc}, yield stress for cortical bone; σ_{yt}, yield stress for trabecular bone

To simulate the experimental setup, the shaft of the simulated femurs was positioned 10º from the horizontal, and the femoral neck was positioned at a 15º internal rotation. The nodes on the surface of the simulated tennis ball on the femoral head were fixed in the loading direction. The nodes on the distal end of the femur were completely fixed. A simulated vertical load was distributed to a pad on the greater trochanter to mimic the experimental setup.

4.4.1 Assessment of hip fracture type (I)

To estimate the experimental fracture type, the principal strain and its distribution at the trabecular bone area were analyzed at seven planes parallel to the femoral neck axis with a distance of 2 mm. The strain thresholds that resulted in uniform strain patterns over the cervical and trochanteric regions were determined. The principal strain threshold ratios ε_C (cervical) and ε_T (trochanteric) were used to assess the fracture type.

For each of the analyzed planes, strain distribution through the cervical and trochanteric regions was tracked by adjusting the strain threshold until the contiguous elements formed a uniform pattern through the neck or trochanter. The strain thresholds that resulted in uniform strain patterns were determined at all the planes. A cervical/trochanteric principal strain threshold ratio $\varepsilon_C/\varepsilon_T > 1.0$ was designated to predict a cervical fracture and $\varepsilon_C/\varepsilon_T < 1.0$ to predict a trochanteric fracture.

4.4.2 Assessment of femoral fracture load (II, III)

Training and validation models

Twenty-one out of the 61 femurs (16 female and 5 male) were used for training, and 40 femurs (25 female and 15 male) were used for validation purposes. The 21 training FE models were used to establish the strain threshold by simulating the experimental loads of the corresponding femurs. The median value of the minimum principal strain was defined as the fracture threshold in compression to be used in the validation set. The 40 validation models were used to estimate the experimental fracture loads.

To test the convergence, models from the training set were generated with maximum element sizes of 2 mm, 3 mm and 4 mm. The models were also used to estimate the sensitivity of the load estimation to the loading direction. The femoral neck was positioned at 0º, 15º and 30º internal rotation angles and the femoral shaft at 10º from the horizontal (Wakao *et al.* 2009). The minimum principal strain was computed and compared between the different loading directions.

The same models were applied to test the influence of the minimum cortical thickness on the minimum principal strain, with the femoral neck positioned at a 15º internal rotation and the femoral shaft positioned 10º from the horizontal. The compared cortical thicknesses were 1 mm, 0.8 mm and 0.6 mm.

Failure criteria

To estimate the experimental fracture load (II, III), nonlinear FE analysis was performed by using the Newton-Raphson method and the Drucker-Prager yield criterion (Drucker & Prager 1952). The mechanical properties were assumed to be bilinearly elastoplastic. A post-yield modulus 5% of the Young's modulus was used (Bayraktar *et al.* 2004). The yielding of an element was determined to occur when the Drucker-Prager equivalent stress exceed the yield stress. The ultimate tensile stress was presumed to be 0.8 times the compressive yield stress. (Bessho *et al.* 2007.) The failure criterion was based on adopting strains in compression and stresses in tension. The training FE models were used to establish the stress and strain thresholds by simulating the experimental loads of the corresponding femurs. In study III, stress threshold in tension was calculated using the following equation

$$\sigma_{Tm} = \varepsilon_{Cm}\left(\frac{\sigma_T}{\varepsilon_C}\right), \quad (4)$$

where σ_T is the maximum principal stress in tension, ε_C is the minimum principal strain in compression and subscript m refers to median. The fracture of the simulated femur was determined to occur when at least one cortical surface element failed in compression or in tension, based on the corresponding threshold values. The element failure thresholds are summarized in Table 6.

Table 6. Summary of the element failure thresholds.

Study	Parameter	Threshold	Description
II	Minimum principal strain	-7,300 microstrain	Using training set models, median
III		-13,500 microstrain	value was defined as the strain threshold.
II	Maximum principal stress	0.8 times the compressive yield stress (MPa)	(Bessho *et al.* 2007)
III		118.6 MPa	The stress threshold was calculated using the training set models.

4.5 Statistical methods

The data were analyzed using SPSS software (versions SPSS 16.0 and IBM SPSS Statistics 20, IBM Corporation, Somers, NY, USA). In all tests, a p-value <0.05 was considered to be statistically significant.

In study I, owing to the limited sample size, Mann-Whitney test was used in group comparisons. The effect of BMD on the difference in strain ratio between fracture types was studied by covariance analysis (ANCOVA) using femoral neck BMD (FNBMD) and trochanteric BMD (TRBMD) as covariates. Receiver operating characteristic (ROC) analysis was used to assess the ability of $\varepsilon_C/\varepsilon_T$ to discriminate cervical and trochanteric hip fractures, and positive predictive values were also calculated.

In studies II and III, linear regression analysis was used to evaluate the relationship between the simulated and the experimentally measured fracture loads, and between BMD and BMC and the fracture loads. Coefficients of determination (r^2) and their 95% confidence intervals (CI) were calculated.

5 Results

5.1 Estimation of experimental fracture type (I)

The FE models resulted in characteristic principal strain distributions for cervical and trochanteric fractures. The principal strain threshold ratio $\varepsilon_C/\varepsilon_T$ in the FE models of femora with experimental cervical fractures (mean ± SD 1.103 ± 0.127) differed significantly ($p = 0.001$) from that in experimental trochanteric fractures (0.925 ± 0.137). The significant difference in the strain ratio between fracture types remained after accounting for FNBMD and TRBMD ($p = 0.014$), showing that it is independent of BMD.

Using the cut-off value of $\varepsilon_C/\varepsilon_T = 1.0$ as criterion, FE model estimated the experimental fracture type correctly in 85% of the cases (12/13 cervical; 10/13 trochanteric fractures). The positive predictive value was 80% (12/15) for cervical fractures and 91% (10/11) for trochanteric fractures. The area under the ROC curve was 0.858 for $\varepsilon_C/\varepsilon_T$ in the discrimination of cervical and trochanteric experimental hip fracture patterns, the sensitivity being 77% with a specificity of 92%.

5.2 Estimation of experimental fracture load (II, III)

Experimental fracture load was estimated using full FE model and cortical bone FE model. Relation between simulated and experimentally measured fracture loads and between BMD and BMC and the fracture loads was analyzed.

5.2.1 Full finite element model (II)

The bilinear elastoplastic FE model accurately estimated the fracture load in the fall under the sideways loading configuration. The estimated fracture load values were significantly correlated with the experimental ones ($r^2 = 0.87$, standard error of the estimate SEE = 392 N, $p < 0.001$) (Fig. 7). The slope was 0.929 (not significantly different from 1, $p = 0.237$), with an intercept of 258 N (not significantly different from 0, $p = 0.239$).

The sensitivity analysis showed that increasing the neck angle from 0º to 15º and from 15º to 30º decreased the absolute value of the minimum principal strain from 3% to 9% and from 6% to 15%, respectively. Decreasing the minimum

cortical thickness from 1 mm to 0.8 mm and from 0.8 mm to 0.6 mm increased the absolute value of the minimum principal strain from 3% to 9% and from 2% to 6%, respectively.

5.2.2 Cortical bone finite element model (III)

The estimated fracture load values were highly correlated with the experimental ones ($r^2 = 0.73$, standard error of the estimate SEE = 558 N, $p < 0.001$) (Fig. 7). The slope was 1.128 (not significantly different from 1, $p = 0.253$), with an intercept of -360 N (not significantly different from 0, $p = 0.362$). The coefficient of determination was $r^2 = 0.68$ for females and $r^2 = 0.70$ for males (Table 7). The corresponding coefficients of determination between BMD and BMC, and the experimental fracture load were $r^2 = 0.41$ (female $r^2 = 0.58$, male $r^2 = 0.05$) and $r^2 = 0.40$ (female $r^2 = 0.62$, male $r^2 = 0.04$), respectively, whereas the coefficient of determination was $r^2 = 0.87$ (female $r^2 = 0.86$, male $r^2 = 0.86$), for the full FE model including trabecular bone (Table 7).

Table 7. Coefficients of determination r^2 and their 95% confidence intervals (CI) between DXA-based BMD and BMC, the cortical FE model and the full FE model including trabecular bone, and the experimental fracture load.

Determinant	All (N = 40)	Female (N = 25)	Male (N = 15)
BMD	0.41 (0.17–0.63)	0.58 (0.28–0.78)	0.05 (0–0.38)
BMC	0.40 (0.13–0.68)	0.62 (0.32–0.84)	0.04 (0–0.40)
Cortical FE model	0.73 (0.57–0.86)	0.68 (0.44–0.89)	0.70 (0.34–0.88)
Full FE model	0.87 (0.79–0.93)	0.86 (0.73–0.94)	0.86 (0.59–0.98)

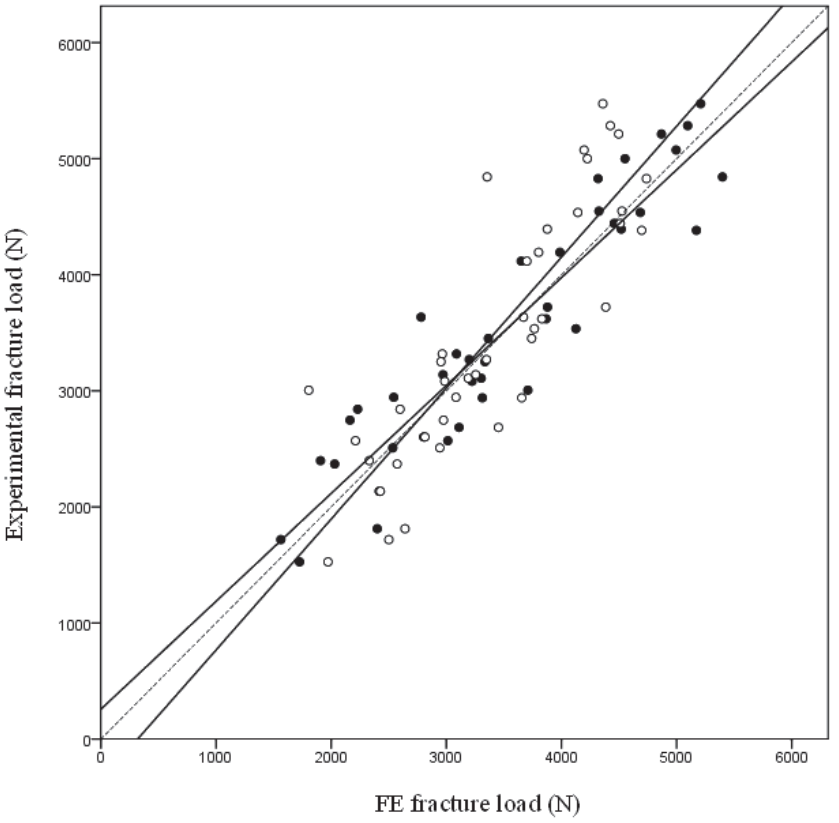

Fig. 7. The relationship between the experimental and FE estimated fracture loads. The filled symbols represent full FE model and the hollow symbols cortical FE model. The solid line represents the linear regression, and the dotted line the function y = x. The slope and intercept was 0.929 and 258 N for the full FE model, whereas it was 1.128 and -360 N for the cortical FE model. The coefficient of determination was r^2 = 0.87 for the full FE model including trabecular bone, and r^2 = 0.73 for the cortical FE model. Loads are given in Newtons (N).

6 Discussion

Hip fracture is a universal health issue, leading to hospitalization and rehabilitation, and at worst, to death. It also leads to high healthcare costs. Therefore, it is necessary to study the methods evaluating the hip fracture risk. The purpose of this study was to develop CT-based FE models to estimate experimental femoral fracture load and hip fracture type in a sideways fall loading configuration. In the estimation of hip fracture type, cervical and trochanteric hip fractures displayed characteristic strain patterns when using a FE model that is mainly driven by bone geometry. This relatively simple FE model estimation provided reasonable agreement for the occurrence of experimental hip fracture type. This study showed that proximal femoral fracture load can be estimated with reasonable accuracy by a relatively simple FE model including only cortical bone. Nevertheless, more accurate assessment of fracture load requires subject-specific modeling, including individual material properties of trabecular bone. Cortical bone FE model was more predictive for fracture load than DXA and slightly less accurate than the subject-specific FE model.

6.1 Finite element methodology (I, II, III)

In study I, a relatively simple geometrical model of the proximal femur with homogenous material properties was used. Hip fracture type was estimated from the principal strain ratio between cervical and trochanteric regions of the femur, which appears to be an effective method when discriminating the experimental hip fracture types. There are few previous studies where hip fracture type is estimated using the CT-based FE model (Bessho *et al.* 2004, Gómez-Benito *et al.* 2005, Keyak *et al.* 2001). In these studies different approaches were used to discriminate fracture types. Gómez-Benito *et al.* (2005) estimated fracture type using anisotropic fracture criterion and coefficient of risk to fracture, while Bessho *et al.* (2004) predicted the fracture type from a crack in the cortical bone, and Keyak *et al.* (2001) used non-surface elements with the lowest factors of safety to predict the experimental fracture site. Heterogeneous material properties for bone were used in these studies.

Since homogeneous material properties for cortical and trabecular bone were used in study I, the strain distributions were mainly influenced by bone geometry. It was shown that with a relatively simple geometry-based model it is possible to estimate the most probable region of fracture with reasonable accuracy. Thus, the

solution to estimate the hip fracture type appeared to be more effective than the approaches used in the previous studies. Even if the model was somewhat simplified compared to patient-specific FE models with individual heterogeneous material properties, it resulted in a good agreement between estimated and detected fracture types, indicating the importance of geometry on fracture mechanics.

In studies II and III, the Drucker-Prager yield criterion was used, because it has been suggested to be more suitable than the von Mises yield criterion in FE models that simulate brittle materials such as bone (Bessho *et al.* 2007). Bessho *et al.* (2007) compared the principal strain, displacement, yield and fracture load of the simulation and the experiment to verify the accuracy of their FE model, attaining realistic fracture load prediction for proximal femurs tested in the stance configuration. It was possible to test this FE method in a different loading setup with our experimental data, where a sideways fall configuration was used. The load case used in studies II and III is related to fragile fractures that are calculated by principal strain or stress. As in the previous study (Bessho *et al.* 2007), the maximum principal stress criteria and the minimum principal strain criteria for element failure in tension and in compression were used, respectively. Similarly, the ultimate tensile stress was presumed to be 0.8 times the compressive yield stress as in the previous study of Bessho *et al.* (2007).

The effect of impact direction and cortical thickness on the fracture load estimation was calculated. The sensitivity analysis showed that the use of a minimum cortical thickness of 1 mm reduces the absolute value of the minimum principal strain in comparison to those for the thinner cortices. The effect of the loading direction with the femoral neck positioned at 0º, 15º and 30º internal rotations and the femoral shaft positioned 10º from the horizontal was tested. Similar positions were used in a previous study of Wakao *et al.* (2009). The results of this previous study were similar to those observed in study II, where estimated load increased with increased internal rotation. Nevertheless, axial loading was not considered, which may have some effect on the results.

For all of the models, separated cortical and trabecular bone compartments were used as previously suggested (Chevalier *et al.* 2009). This enabled the estimation of experimental fracture load of the proximal femur using only cortical bone in the FE models in study III. Due to the somewhat high sample size, it was possible to use a set of training models to establish the specific stress and strain thresholds. To optimize the models, the median values of the training set were applied for the strain thresholds in each model. The strain threshold in

compression in study III was -13,500 microstrain for the cortical bone training models, whereas it was -7,300 microstrain in the training models of study II including both cortical and trabecular bone. In contrast, Bessho *et al.* (2007) used a principal strain threshold value of -10,000 microstrain as the failure criterion for element in compression. Nevertheless, the failure criteria based on training sets of studies II and III appeared to result in a reasonable accuracy of the fracture load in both validation sets. Based on the results of these studies, it seems that the selected failure criterion was effective for our study sample, and the Drucker-Prager method is applicable also for a sideways fall load configuration.

All studies had somewhat similar limitations. Only cadaver femurs were used and the *in vivo* conditions were not modeled. A limited spatial resolution of the CT data was used to restrict the size of the FE model. More accurate information might be available with a FE model with more elements and material properties covering each cortical element separately and which uses more accurate cortical density and cortical thickness values instead of the constant density and adjusted minimum thickness of 1 mm that were used in this study. The distal proximal femur was free to rotate around an axis in the experimental setup, whereas it was constrained in the FE model. This results in some inaccuracy in the stress-strain distribution in the models. Experimentally measured strain values were not available, and no comparison was made between experimental and FE estimated strains. Parametric analysis was not conducted for the FE models. The effect of formalin fixation on the measured parameters was not studied. Previously, Sedlin and Hirsch (1966) found no significant difference in Young's modulus in tension between formalin-fixed and non-fixed cortical specimens. However, in the more recent study of Öhman *et al.* (2008) no effect of formalin fixation on the yield stress, the ultimate stress or the hardness of human cortical bone was found, whereas 8-week storage decreased the Young's modulus and increased yield and ultimate strain. Nevertheless, the use of fresh-frozen bone specimens is recommended in biomechanical studies because plastic mechanical properties may alter significantly during long-term fixation (Unger *et al.* 2010). Either way, caution should be exercised when interpreting the results from the FE model, as it is calibrated against formalin-fixed specimens. In addition to these shared limitations, trabecular bone was assumed as a continuum and no sensitivity analysis was performed in study I, and no comparison with actual yield loads was made due to the lack of experimentally measured yield load values in studies II and III. Furthermore, trabecular bone was not removed from the actual femurs

and no comparison of fracture loads between FE cortical bone and experimental cortical bone was made in study III.

6.2 Assessment of hip fracture type (I)

Since homogeneous material properties for bone were used in study I, the strain distributions were mainly influenced by bone geometry. This supports the suggestions that femurs with different fracture types differ geometrically and have different failure mechanisms, and the risk for different fracture types should be estimated separately (Gnudi *et al.* 2002, Mautalen *et al.* 1996, Pulkkinen *et al.* 2006, Partanen *et al.* 2001).

Bone geometry that comprises e.g. femoral neck axis length (FNAL) or hip axis length (HAL), femoral neck-shaft angle (NSA) and cortical thickness, varies between fracture types (Gnudi *et al.* 2002, Pulkkinen *et al.* 2004, Pulkkinen *et al.* 2006, Bergot *et al.* 2002). The most important geometric parameters to assess the risk for a specific fracture type are NSA and cortical thickness at the femoral shaft (FSC) or calcar femoralis (CFC) when assessed from two-dimensional projection images (Pulkkinen *et al.* 2004, Partanen *et al.* 2001). The effect of these parameters on the femoral stress-strain distribution is suggested to be important (Voo *et al.* 2004). The results of study I support the previous studies, showing that upper femur geometry contributes to strain distribution, and consequently, to the fracture type.

In study I, 12 out of 13 cervical fracture cases were correctly estimated. This result is supported by the previous studies, where cervical fractures were suggested to be mainly determined by bone geometry (Gnudi *et al.* 2002, Pulkkinen *et al.* 2004, Pulkkinen *et al.* 2006). In contrast to cervical fractures, the model was incapable of estimating the fracture type correctly in 3 of 13 experimental trochanteric fracture cases.

Previous studies have suggested that trochanteric fractures are largely determined by BMD (Pulkkinen *et al.* 2004, Schott *et al.* 1998, Schott *et al.* 2005). Trochanteric failure occurs preferably with high fracture load levels, while fracture of the femoral neck is more common in femora with lower bone strength (Pulkkinen *et al.* 2004). The data presented in study I seem to support this finding, BMD for the trochanteric fractures being generally higher than those for the femoral neck fractures. Homogenous material properties were used and variations in bone density were not included in the FE models. The study was aimed to test the hypothesis that individual proximal femur geometry results in strain

distribution that coincides with fracture type. With a relatively simple geometry-based model, it was possible to estimate accurately the most probable region of fracture.

The few previous studies estimating the hip fracture type with CT-based FE model (Bessho *et al.* 2004, Gómez-Benito *et al.* 2005, Keyak *et al.* 2001) used different approaches to discriminate fracture types, and only Keyak *et al.* (2001) truly compared the experimental and the FE-predicted hip fracture type. With their FE model estimations in a fall loading configuration, 67% agreement for the occurrence of experimental hip fracture type was achieved. The estimated and the experimental fracture type matched in 10 out of 15 cases. In study I, the fracture type was estimated correctly in 22 of the 26 cases, giving a prediction accuracy of 85% for the occurrence of experimental hip fracture type. The FE model used in study I was rather simple compared with patient-specific models, and the solution to estimate the hip fracture type appeared to be rather effective.

6.3 Assessment of femoral fracture load (II, III)

In study II, a CT-based bilinear elastoplastic FE model that estimated the fracture load of formalin-fixed proximal femora was created. This model formed a basis of the cortical bone model that was generated in study III. Trabecular bone was removed from the models and only cortical bone was modeled. The cortical model was more predictive for fracture load than DXA-based BMD or BMC. The separate correlation analysis for male and female subjects (Table 7) shows that the model is somewhat equally good at predicting fracture load in both genders, and the benefits compared to BMD and BMC measures are still maintained. Furthermore, this approach was computationally more effective and it was only slightly less accurate than a full bone FE model which accurately estimated experimentally measured fracture load values of the sideways loading configuration in study II. The calculation time of the cortical bone models was less than quarter of an hour, while it was multiple hours for a similar model with trabecular bone. The correlation between the FE model and experimental load obtained in study III is well compatible with that in study II, suggesting that cortical bone can largely explain the fracture load of a proximal femur during a fall to the side. This is supported by previous studies (Holzer *et al.* 2009, de Bakker *et al.* 2009), where it was found that bone strength depends mostly on cortical bone. Holzer *et al.* (2009) prepared eighteen paired human cadaver femurs so that trabecular bone was completely removed from the femoral neck of

one bone of the pair, thus providing one full bone and another without trabecular structure. The prepared femora were mechanically tested using a model shown to produce reproducible femoral neck fractures (Kukla *et al.* 2002). In addition, it has been suggested that most of the load transfers through cortical structure and trabecular bone mainly reinforce cortical bone (de Bakker *et al.* 2009). This agrees with FE data provided in study III in a similar loading configuration, where a good correlation was found between the estimated and experimental fracture load.

The results of study II (slope = 0.929, intercept = 258 N, SEE = 392 N, r = 0.931) show that the model can accurately explain the fracture load with a slope close to 1 and a relatively small intercept. Previously, Keyak (2001) achieved improved prediction of femoral fracture load using nonlinear FE model, and reported that the slope and intercept of the regression line for the relationship between the FE-computed fracture load values and the measured fracture load values were 0.77 and 1150 N (SEE = 830 N, r = 0.962, N = 18), respectively, with the one-leg stance loading configuration. In their study, Bessho *et al.* (2007) reported values of 0.936 and 641 N (SEE = 228 N, r = 0.979, N = 11) for the slope and intercept, respectively. However, a sideways fall configuration instead of a stance configuration was used in studies II and III. This kind of loading setup represents an unprotected sideways fall onto the hip (Greenspan *et al.* 1998) associated with the majority of hip fractures (Parkkari *et al.* 1999).

There are some previous FE studies that estimate experimental fracture load in a configuration that simulates a fall to the side (Dragomir-Daescu *et al.* 2011, Keyak *et al.* 1998, Lotz *et al.* 1991a, Lotz *et al.* 1991b). However, the boundary conditions and positioning of the femur were different in the studies. Lotz *et al.* limited their FE study to only one femur for the sideways fall configuration (Lotz *et al.* 1991a, Lotz *et al.* 1991b). Keyak *et al.* (1998) used a factor of safety for elements to predict femoral fracture load. The factor of safety was calculated by dividing element strength with element von Mises stress. They reported that the measured and FE-predicted fracture loads were nonlinearly related (measured fracture load = 1.24 FE predicted fracture load 1.22, SEE = 0.0909 log10 kN, r = 0.949, N = 18). Dragomir-Daescu *et al.* (2011) determined element failure to take place when von Mises strain exceeds the yield strain. They attained values of 1.42 and 995.87 N (r = 0.964, N = 9) for training set slope and intercept, respectively. For their validation set, the corresponding values were 1.36 and 580.04 N (r = 0.927, N = 9). Thus, our results are in good agreement with previous literature.

In most of these studies using a fall configuration, bone strength was directly estimated, without first assessing the accuracy in strain estimation. As mentioned earlier in the text, this is also a limitation of this study. There are few studies in which high *in vitro* strain prediction accuracy was found when comparing experimental and FE-based strains in axial loading conditions (Bessho *et al.* 2007, Schileo *et al.* 2007, Trabelsi *et al.* 2009) and in a sideways loading configuration (Grassi *et al.* 2012). Improved strain predictions have also been reported (Schileo *et al.* 2008, Trabelsi *et al.* 2011). This is indeed an important issue when validating a simulation model to assess hip fracture risk. Experimental data including strain measurements for the femur are a valuable asset, providing state-of-the-art framework for the validation of a FE model. For this study, strain gauges were not used in the experimental setup, and strain values were not available. However, because of the somewhat large sample size, it was possible to use training and validation sets when estimating the femoral fracture load. The training FE models were used to attain the strain threshold by simulating the experimental loads of the corresponding femurs. Based on the results of study II, it seems that the selected failure criterion was effective for our study sample, and the femoral fracture load was estimated with good accuracy by using the CT-based bilinear elastoplastic FE model.

6.4 Comparison of the finite element models (I, II, III)

The approaches for the models that estimate hip fracture type (I) and femoral fracture load (II, III) differ in the present study. Compared with the detailed semi-automatic segmentation (II, III), manual segmentation (I) might produce some inaccuracies to the bone shape due to operator error. In study I, trabecular bone was also assumed as a continuum, and bilinear elastoplastic analysis was not considered as opposed to studies II and III. Fracture criteria also differed so that the fracture was estimated more locally in studies II and III. The models in studies I and III are considerably faster to compute than the model in study II, which provided an accurate but not an effective solution.

Although the approaches differ between the models, it might be possible to use these models as a tool to develop an integrated model, in which some properties from all three models are merged, to find an optimal model for clinical use. The cortical bone model (III) was more predictive for fracture load than DXA and slightly less accurate than a full-bone FE model including trabecular bone. Still, the accuracy leaves little to be desired. Taking all the three models into

consideration, one approach for optimization might be for example bilinear elastoplastic model with homogenous material properties for trabecular bone, which might be enough for an accurate and rapid assessment of hip fracture risk. In addition to quick analysis, generation of the model would have to be more automated for effective clinical use.

6.5 Prospects for finite element modeling of bone

One major limitation of CT-based methods in FE modeling *in vivo* is the radiation dose. Typically a compromise has to be made between accuracy and the radiation exposure of the CT scan. Low radiation dose methods, such as volumetric dual X-ray absorptiometry (VXA), and advanced algorithms for CT, are under development. At the same time, FE modeling of bone is moving towards the generation of three-dimensional models from two-dimensional data. It remains to be seen which one of these contemporary trends results in a more effective tool for evaluating fracture risk, or whether it is a combination of methods that will govern the progress of the field. Nevertheless, the results of this study suggest that high resolution might not even be needed to achieve good prediction accuracy in the assessment of hip fracture risk. Computationally effective simplified models with reduced properties estimated the femoral fracture load and hip fracture type with reasonable accuracy *in vitro*. Although the adequate results and the short calculation time are promising in view of effective use of the models, this study was based on experimental data, and the results should be verified in a prospective clinical study. Recently, FE analysis has been used in a few clinical studies (Amin *et al.* 2011, Keaveny *et al.* 2010, Lewiecki *et al.* 2009), which support the notion that CT-based biomechanical FE modeling is a powerful tool to estimate whole-bone strength *in vivo*, and can thus be applied also in a clinical environment.

7 Conclusions

Hip fracture is a major problem in health care, which is why it is necessary to study fracture mechanisms and develop improved methods estimating individual fracture risk. In this study, computed tomography-based finite element methods were investigated and simulation models developed to estimate experimental femoral fracture load and hip fracture type in a sideways fall loading configuration.

In the estimation of hip fracture type, cervical and trochanteric hip fractures displayed characteristic strain patterns when using a FE model mainly driven by bone geometry. This relatively simple FE model estimation provided reasonable agreement for the occurrence of experimental hip fracture type.

This study showed that proximal femoral fracture load can be estimated with reasonable accuracy by a relatively simple FE model including only cortical bone. However, more accurate assessment of fracture load requires subject-specific modeling, including individual material properties of trabecular bone for bilinear elastoplastic FE models. Based on the aims of this study, it can be concluded that:

1. Cervical and trochanteric hip fractures display characteristic strain patterns. Cervical vs. trochanteric region principal strain ratio $\varepsilon_C/\varepsilon_T$ differs significantly between femora with cervical vs. trochanteric fracture.
2. It is possible to estimate fracture load with relatively high accuracy with subject-specific bilinear elastoplastic FE models.
3. Cortical bone FE model is more predictive for fracture load than DXA and only slightly less accurate than a full-bone FE model including trabecular bone.

References

Amin S, Kopperdhal DL, Melton LJ,3rd, Achenbach SJ, Therneau TM, Riggs BL, Keaveny TM & Khosla S (2011) Association of hip strength estimates by finite-element analysis with fractures in women and men. J Bone Miner Res 26(7): 1593–1600.

Angelsen B (2000) Ultrasound imaging: Waves, signals and signal processing. Trondheim, Emantec.

Barkmann R, Dencks S, Laugier P, Padilla F, Brixen K, Ryg J, Seekamp A, Mahlke L, Bremer A, Heller M & Glüer CC (2010) Femur ultrasound (FemUS)--first clinical results on hip fracture discrimination and estimation of femoral BMD. Osteoporos Int 21(6): 969–976.

Bayraktar HH, Morgan EF, Niebur GL, Morris GE, Wong EK & Keaveny TM (2004) Comparison of the elastic and yield properties of human femoral trabecular and cortical bone tissue. J Biomech 37(1): 27–35.

Benhamou CL, Poupon S, Lespessailles E, Loiseau S, Jennane R, Siroux V, Ohley W & Pothuaud L (2001) Fractal analysis of radiographic trabecular bone texture and bone mineral density: two complementary parameters related to osteoporotic fractures. J Bone Miner Res 16(4): 697–704.

Bergot C, Bousson V, Meunier A, Laval-Jeantet M & Laredo JD (2002) Hip fracture risk and proximal femur geometry from DXA scans. Osteoporos Int 13(7): 542–550.

Bessho M, Ohnishi I, Matsuyama J, Matsumoto T, Imai K & Nakamura K (2007) Prediction of strength and strain of the proximal femur by a CT-based finite element method. J Biomech 40(8): 1745–1753.

Bessho M, Ohnishi I, Okazaki H, Sato W, Kominami H, Matsunaga S & Nakamura K (2004) Prediction of the strength and fracture location of the femoral neck by CT-based finite-element method: a preliminary study on patients with hip fracture. J Orthop Sci 9(6): 545–550.

Bousson V, Le Bras A, Roqueplan F, Kang Y, Mitton D, Kolta S, Bergot C, Skalli W, Vicaut E, Kalender W, Engelke K & Laredo JD (2006) Volumetric quantitative computed tomography of the proximal femur: relationships linking geometric and densitometric variables to bone strength. Role for compact bone. Osteoporos Int 17(6): 855–864.

Bouxsein ML, Courtney AC & Hayes WC (1995) Ultrasound and densitometry of the calcaneus correlate with the failure loads of cadaveric femurs. Calcif Tissue Int 56(2): 99–103.

Braithwaite RS, Col NF & Wong JB (2003) Estimating hip fracture morbidity, mortality and costs. J Am Geriatr Soc 51(3): 364–370.

Casper DS, Kim GK, Parvizi J & Freeman TA (2012) Morphology of the proximal femur differs widely with age and sex: relevance to design and selection of femoral prostheses. J Orthop Res 30(7): 1162–1166.

Cefalu CA (2004) Is bone mineral density predictive of fracture risk reduction? Curr Med Res Opin 20(3): 341–349.

Chappard C, Bousson V, Bergot C, Mitton D, Marchadier A, Moser T, Benhamou CL & Laredo JD (2010) Prediction of femoral fracture load: cross-sectional study of texture analysis and geometric measurements on plain radiographs versus bone mineral density. Radiology 255(2): 536–543.

Chevalier Y, Pahr D & Zysset PK (2009) The role of cortical shell and trabecular fabric in finite element analysis of the human vertebral body. J Biomech Eng 131(11): 111003.

Cordey J & Gautier E (1999) Strain gauges used in the mechanical testing of bones. Part I: Theoretical and technical aspects. Injury 30 Suppl 1: A7–13.

Coupland C, Wood D & Cooper C (1993) Physical inactivity is an independent risk factor for hip fracture in the elderly. J Epidemiol Community Health 47(6): 441–443.

Courtney AC, Wachtel EF, Myers ER & Hayes WC (1994) Effects of loading rate on strength of the proximal femur. Calcif Tissue Int 55(1): 53–58.

Courtney AC, Wachtel EF, Myers ER & Hayes WC (1995) Age-related reductions in the strength of the femur tested in a fall-loading configuration. J Bone Joint Surg Am 77(3): 387–395.

Cummings R & Klineberg R (1994) Fall frequency and characteristics and the risk of hip fractures. J Am Geriatr Soc 42(7): 774–778.

Cummings SR & Melton LJ (2002) Epidemiology and outcomes of osteoporotic fractures. Lancet 359(9319): 1761–1767.

Cummings SR, Nevitt MC, Browner WS, Stone K, Fox KM, Ensrud KE, Cauley J, Black D & Vogt TM (1995) Risk factors for hip fracture in white women. Study of Osteoporotic Fractures Research Group. N Engl J Med 332(12): 767–773.

Currey J (2002) Bones: Structure and mechanics. Princeton, NJ, Princeton University Press.

Dalén N, Hellström LG & Jacobson B (1976) Bone mineral content and mechanical strength of the femoral neck. Acta Orthop Scand 47(5): 503–508.

Dargent-Molina P, Favier F, Grandjean H, Baudoin C, Schott AM, Hausherr E, Meunier PJ & Bréart G (1996) Fall-related factors and risk of hip fracture: the EPIDOS prospective study. Lancet 348(9021): 145–149.

de Bakker PM, Manske SL, Ebacher V, Oxland TR, Cripton PA & Guy P (2009) During sideways falls proximal femur fractures initiate in the superolateral cortex: evidence from high-speed video of simulated fractures. J Biomech 42(12): 1917–1925.

Dempster DW (2003) Bone microarchitecture and strength. Osteoporos Int 14 Suppl 5: S54–56.

Donnelly E (2011) Methods for assessing bone quality: a review. Clin Orthop Relat Res 469(8): 2128–2138.

Dragomir-Daescu D, Op Den Buijs J, McEligot S, Dai Y, Entwistle RC, Salas C, Melton LJ,3rd, Bennet KE, Khosla S & Amin S (2011) Robust QCT/FEA models of proximal femur stiffness and fracture load during a sideways fall on the hip. Ann Biomed Eng 39(2): 742–755.

Drucker D & Prager W (1952) Soil mechanics and plastic analysis for limit design. Quart Appl Math 10(2): 157–165.

Duboeuf F, Hans D, Schott AM, Kotzki PO, Favier F, Marcelli C, Meunier PJ & Delmas PD (1997) Different morphometric and densitometric parameters predict cervical and trochanteric hip fracture: the EPIDOS Study. J Bone Miner Res 12(11): 1895–1902.

Eckstein F, Wunderer C, Boehm H, Kuhn V, Priemel M, Link TM & Lochmüller EM (2004) Reproducibility and side differences of mechanical tests for determining the structural strength of the proximal femur. J Bone Miner Res 19(3): 379–385.

Enoka R (2002) Neuromechanics of human movement. Champaign, IL, Human Kinetics.

Frost HM (1987) Bone "mass" and the "mechanostat": a proposal. Anat Rec 219(1): 1–9.

Frost HM (1994) Wolff's Law and bone's structural adaptations to mechanical usage: an overview for clinicians. Angle Orthod 64(3): 175–188.

Frost HM (1997) On our age-related bone loss: insights from a new paradigm. J Bone Miner Res 12(10): 1539–1546.

Genant HK, Engelke K & Prevrhal S (2008) Advanced CT bone imaging in osteoporosis. Rheumatology (Oxford) 47 Suppl 4: iv9–16.

Gnudi S, Ripamonti C, Lisi L, Fini M, Giardino R & Giavaresi G (2002) Proximal femur geometry to detect and distinguish femoral neck fractures from trochanteric fractures in postmenopausal women. Osteoporos Int 13(1): 69–73.

Gómez-Benito MJ, García-Aznar JM & Doblaré M (2005) Finite element prediction of proximal femoral fracture patterns under different loads. J Biomech Eng 127(1): 9–14.

Grassi L, Schileo E, Taddei F, Zani L, Juszczyk M, Cristofolini L & Viceconti M (2012) Accuracy of finite element predictions in sideways load configurations for the proximal human femur. J Biomech 45(2): 394–399.

Greenspan SL, Myers ER, Kiel DP, Parker RA, Hayes WC & Resnick NM (1998) Fall direction, bone mineral density, and function: risk factors for hip fracture in frail nursing home elderly. Am J Med 104(6): 539–545.

Gregory JS, Testi D, Stewart A, Undrill PE, Reid DM & Aspden RM (2004) A method for assessment of the shape of the proximal femur and its relationship to osteoporotic hip fracture. Osteoporos Int 15(1): 5–11.

Hans D & Krieg MA (2008) The clinical use of quantitative ultrasound (QUS) in the detection and management of osteoporosis. IEEE Trans Ultrason Ferroelectr Freq Control 55(7): 1529–1538.

Hayes WC, Myers ER, Robinovitch SN, Van Den Kroonenberg A, Courtney AC & McMahon TA (1996) Etiology and prevention of age-related hip fractures. Bone 18(1 Suppl): 77S-86S.

Holzer G, von Skrbensky G, Holzer LA & Pichl W (2009) Hip fractures and the contribution of cortical versus trabecular bone to femoral neck strength. J Bone Miner Res 24(3): 468–474.

Huber MB, Carballido-Gamio J, Fritscher K, Schubert R, Haenni M, Hengg C, Majumdar S & Link TM (2009) Development and testing of texture discriminators for the analysis of trabecular bone in proximal femur radiographs. Med Phys 36(11): 5089–5098.

Ito M (2011) Recent progress in bone imaging for osteoporosis research. J Bone Miner Metab 29(2): 131–140.

Iwamoto J, Sato Y, Takeda T & Matsumoto H (2009) Role of sport and exercise in the maintenance of female bone health. J Bone Miner Metab 27(5): 530–537.

Jee W (2001) Integrated bone tissue physiology: Anatomy and physiology. In Cowin S (ed) Bone mechanics handbook. New York, NY, Informa Healthcare.

Johnell O & Kanis JA (2006) An estimate of the worldwide prevalence and disability associated with osteoporotic fractures. Osteoporos Int 17(12): 1726–1733.

Kaneko TS, Pejcic MR, Tehranzadeh J & Keyak JH (2003) Relationships between material properties and CT scan data of cortical bone with and without metastatic lesions. Med Eng Phys 25(6): 445–454.

Kanis JA (1994) Assessment of fracture risk and its application to screening for postmenopausal osteoporosis: synopsis of a WHO report. WHO Study Group. Osteoporos Int 4(6): 368–381.

Kanis JA (2002) Diagnosis of osteoporosis and assessment of fracture risk. Lancet 359(9321): 1929–1936.

Kanis JA, Johnell O, Oden A, Johansson H & McCloskey E (2008) FRAX and the assessment of fracture probability in men and women from the UK. Osteoporos Int 19(4): 385–397.

Kanis JA, Johnell O, Oden A, Jonsson B, De Laet C & Dawson A (2000) Risk of hip fracture according to the World Health Organization criteria for osteopenia and osteoporosis. Bone 27(5): 585–590.

Kanis JA, Melton LJ,3rd, Christiansen C, Johnston CC & Khaltaev N (1994) The diagnosis of osteoporosis. J Bone Miner Res 9(8): 1137–1141.

Kanis JA, Oden A, Johnell O, Jonsson B, de Laet C & Dawson A (2001) The burden of osteoporotic fractures: a method for setting intervention thresholds. Osteoporos Int 12(5): 417–427.

Kannus P, Niemi S, Parkkari J, Palvanen M, Vuori I & Järvinen M (2006) Nationwide decline in incidence of hip fracture. J Bone Miner Res 21(12): 1836–1838.

Karlsson KM, Sernbo I, Obrant KJ, Redlund-Johnell I & Johnell O (1996) Femoral neck geometry and radiographic signs of osteoporosis as predictors of hip fracture. Bone 18(4): 327–330.

Keaveny TM, Kopperdahl DL, Melton LJ,3rd, Hoffmann PF, Amin S, Riggs BL & Khosla S (2010) Age-dependence of femoral strength in white women and men. J Bone Miner Res 25(5): 994–1001.

Keyak JH (2001) Improved prediction of proximal femoral fracture load using nonlinear finite element models. Med Eng Phys 23(3): 165–173.

Keyak JH, Lee IY & Skinner HB (1994) Correlations between orthogonal mechanical properties and density of trabecular bone: use of different densitometric measures. J Biomed Mater Res 28(11): 1329–1336.

Keyak JH & Rossi SA (2000) Prediction of femoral fracture load using finite element models: an examination of stress- and strain-based failure theories. J Biomech 33(2): 209–214.

Keyak JH, Rossi SA, Jones KA, Les CM & Skinner HB (2001) Prediction of fracture location in the proximal femur using finite element models. Med Eng Phys 23(9): 657–664.

Keyak JH, Rossi SA, Jones KA & Skinner HB (1998) Prediction of femoral fracture load using automated finite element modeling. J Biomech 31(2): 125–133.

Krieg MA, Cornuz J, Ruffieux C, Van Melle G, Büche D, Dambacher MA, Hans D, Hartl F, Häuselmann HJ, Kraenzlin M, Lippuner K, Neff M, Pancaldi P, Rizzoli R, Tanzi F, Theiler R, Tyndall A, Wimpfheimer C & Burckhardt P (2006) Prediction of hip fracture risk by quantitative ultrasound in more than 7000 Swiss women > or =70 years of age: comparison of three technologically different bone ultrasound devices in the SEMOF study. J Bone Miner Res 21(9): 1457–1463.

Kukla C, Gaebler C, Pichl RW, Prokesch R, Heinze G & Heinz T (2002) Predictive geometric factors in a standardized model of femoral neck fracture. Experimental study of cadaveric human femurs. Injury 33(5): 427–433.

Lau KH & Baylink DJ (1999) Vitamin D therapy of osteoporosis: plain vitamin D therapy versus active vitamin D analog (D-hormone) therapy. Calcif Tissue Int 65(4): 295–306.

Leib ES, Lewiecki EM, Binkley N, Hamdy RC & International Society for Clinical Densitometry (2004) Official positions of the International Society for Clinical Densitometry. J Clin Densitom 7(1): 1–6.

Lengsfeld M, Schmitt J, Alter P, Kaminsky J & Leppek R (1998) Comparison of geometry-based and CT voxel-based finite element modelling and experimental validation. Med Eng Phys 20(7): 515–522.

Lewiecki EM, Keaveny TM, Kopperdahl DL, Genant HK, Engelke K, Fuerst T, Kivitz A, Davies RY & Fitzpatrick LA (2009) Once-monthly oral ibandronate improves biomechanical determinants of bone strength in women with postmenopausal osteoporosis. J Clin Endocrinol Metab 94(1): 171–180.

Lindsay R (1994) Prevention of osteoporosis. Prev Med 23(5): 722–726.

Lochmüller EM, Groll O, Kuhn V & Eckstein F (2002) Mechanical strength of the proximal femur as predicted from geometric and densitometric bone properties at the lower limb versus the distal radius. Bone 30(1): 207–216.

Logan D (2007) A first course in the finite element method. Toronto, Ontario, Nelson.

Lotz JC, Cheal EJ & Hayes WC (1991a) Fracture prediction for the proximal femur using finite element models: Part I--Linear analysis. J Biomech Eng 113(4): 353–360.

Lotz JC, Cheal EJ & Hayes WC (1991b) Fracture prediction for the proximal femur using finite element models: Part II--Nonlinear analysis. J Biomech Eng 113(4): 361–365.

Lotz JC, Cheal EJ & Hayes WC (1995) Stress distributions within the proximal femur during gait and falls: implications for osteoporotic fracture. Osteoporos Int 5(4): 252–261.

Majumdar S, Genant HK, Grampp S, Newitt DC, Truong VH, Lin JC & Mathur A (1997) Correlation of trabecular bone structure with age, bone mineral density, and osteoporotic status: in vivo studies in the distal radius using high resolution magnetic resonance imaging. J Bone Miner Res 12(1): 111–118.

Majumder S, Roychowdhury A & Pal S (2008) Effects of trochanteric soft tissue thickness and hip impact velocity on hip fracture in sideways fall through 3D finite element simulations. J Biomech 41(13): 2834–2842.

Marcus R (1989) Understanding and preventing osteoporosis. Hosp Pract (Off Ed) 24(4): 189–204, 209–11, 215 passim.

Marshall D, Johnell O & Wedel H (1996) Meta-analysis of how well measures of bone mineral density predict occurrence of osteoporotic fractures. BMJ 312(7041): 1254–1259.

Mautalen CA, Vega EM & Einhorn TA (1996) Are the etiologies of cervical and trochanteric hip fractures different? Bone 18(3 Suppl): 133S–137S.

Müller ME & Nazarian S (1981) Classification of fractures of the femur and its use in the A.O. index (author's transl). Rev Chir Orthop Reparatrice Appar Mot 67(3): 297–309.

Nurmi I, Narinen A, Lüthje P & Tanninen S (2003) Cost analysis of hip fracture treatment among the elderly for the public health services: a 1-year prospective study in 106 consecutive patients. Arch Orthop Trauma Surg 123(10): 551–554.

Öhman C, Dall'Ara E, Baleani M, Van Sint Jan S & Viceconti M (2008) The effects of embalming using a 4% formalin solution on the compressive mechanical properties of human cortical bone. Clin Biomech (Bristol, Avon) 23(10): 1294–1298.

Parfitt A (2009) Skeletal heterogeneity and the purposes of bone remodelling: Implications for the understanding of osteoporosis. In Marcus R, Feldman D, Nelson D & Rosen C (eds) Fundamentals of osteoporosis. Burlington, MA, Academic Press.

Parker M & Johansen A (2006) Hip fracture. BMJ 333(7557): 27–30.

Parker MJ & Twemlow TR (1997) Spontaneous hip fractures, 44/872 in a prospective study. Acta Orthop Scand 68(4): 325–326.

Parkkari J, Kannus P, Palvanen M, Natri A, Vainio J, Aho H, Vuori I & Järvinen M (1999) Majority of hip fractures occur as a result of a fall and impact on the greater trochanter of the femur: a prospective controlled hip fracture study with 206 consecutive patients. Calcif Tissue Int 65(3): 183–187.

Partanen J, Jämsä T & Jalovaara P (2001) Influence of the upper femur and pelvic geometry on the risk and type of hip fractures. J Bone Miner Res 16(8): 1540–1546.

Peacock M (1998) Effects of calcium and vitamin D insufficiency on the skeleton. Osteoporos Int 8 Suppl 2: S45–51.

Peng L, Bai J, Zeng X & Zhou Y (2006) Comparison of isotropic and orthotropic material property assignments on femoral finite element models under two loading conditions. Med Eng Phys 28(3): 227–233.

Pulkkinen P, Eckstein F, Lochmüller EM, Kuhn V & Jämsä T (2006) Association of geometric factors and failure load level with the distribution of cervical vs. trochanteric hip fractures. J Bone Miner Res 21(6): 895–901.

Pulkkinen P, Glüer CC & Jämsä T (2011) Investigation of differences between hip fracture types: a worthy strategy for improved risk assessment and fracture prevention. Bone 49(4): 600–604.

Pulkkinen P, Jämsä T, Lochmüller EM, Kuhn V, Nieminen MT & Eckstein F (2008) Experimental hip fracture load can be predicted from plain radiography by combined analysis of trabecular bone structure and bone geometry. Osteoporos Int 19(4): 547–558.

Pulkkinen P, Partanen J, Jalovaara P & Jämsä T (2004) Combination of bone mineral density and upper femur geometry improves the prediction of hip fracture. Osteoporos Int 15(4): 274–280.

Pulkkinen P, Partanen J, Jalovaara P & Jämsä T (2010) BMD T-score discriminates trochanteric fractures from unfractured controls, whereas geometry discriminates cervical fracture cases from unfractured controls of similar BMD. Osteoporos Int 21(7): 1269–1276.

Reis J, Silva F, Queiroga C, Lucena S & Potes J (2011) Bone mechanotransduction: A review. JBB 2(1): 37–44.

Rho JY, Kuhn-Spearing L & Zioupos P (1998) Mechanical properties and the hierarchical structure of bone. Med Eng Phys 20(2): 92–102.

Richelson LS, Wahner HW, Melton LJ,3rd & Riggs BL (1984) Relative contributions of aging and estrogen deficiency to postmenopausal bone loss. N Engl J Med 311(20): 1273–1275.

Rizzoli R, Bruyere O, Cannata-Andia JB, Devogelaer JP, Lyritis G, Ringe JD, Vellas B & Reginster JY (2009) Management of osteoporosis in the elderly. Curr Med Res Opin 25(10): 2373–2387.

Schiessl H, Frost HM & Jee WS (1998) Estrogen and bone-muscle strength and mass relationships. Bone 22(1): 1–6.

Schileo E, Dall'Ara E, Taddei F, Malandrino A, Schotkamp T, Baleani M & Viceconti M (2008) An accurate estimation of bone density improves the accuracy of subject-specific finite element models. J Biomech 41(11): 2483–2491.

Schileo E, Taddei F, Malandrino A, Cristofolini L & Viceconti M (2007) Subject-specific finite element models can accurately predict strain levels in long bones. J Biomech 40(13): 2982–2989.

Schott AM, Cormier C, Hans D, Favier F, Hausherr E, Dargent-Molina P, Delmas PD, Ribot C, Sebert JL, Breart G & Meunier PJ (1998) How hip and whole-body bone mineral density predict hip fracture in elderly women: the EPIDOS Prospective Study. Osteoporos Int 8(3): 247–254.

Schott AM, Hans D, Duboeuf F, Dargent-Molina P, Hajri T, Breart G, Meunier PJ & EPIDOS Study Group (2005) Quantitative ultrasound parameters as well as bone mineral density are better predictors of trochanteric than cervical hip fractures in elderly women. Results from the EPIDOS study. Bone 37(6): 858–863.

Schott AM, Weill-Engerer S, Hans D, Duboeuf F, Delmas PD & Meunier PJ (1995) Ultrasound discriminates patients with hip fracture equally well as dual energy X-ray absorptiometry and independently of bone mineral density. J Bone Miner Res 10(2): 243–249.

Schuit SC, van der Klift M, Weel AE, de Laet CE, Burger H, Seeman E, Hofman A, Uitterlinden AG, van Leeuwen JP & Pols HA (2004) Fracture incidence and association with bone mineral density in elderly men and women: the Rotterdam Study. Bone 34(1): 195–202.

Sedlin ED & Hirsch C (1966) Factors affecting the determination of the physical properties of femoral cortical bone. Acta Orthop Scand 37(1): 29–48.

Seeman E & Delmas PD (2006) Bone quality--the material and structural basis of bone strength and fragility. N Engl J Med 354(21): 2250–2261.

Singh M, Nagrath AR & Maini PS (1970) Changes in trabecular pattern of the upper end of the femur as an index of osteoporosis. J Bone Joint Surg Am 52(3): 457–467.

Stewart A, Kumar V & Reid DM (2006) Long-term fracture prediction by DXA and QUS: a 10-year prospective study. J Bone Miner Res 21(3): 413–418.

Stone KL, Seeley DG, Lui LY, Cauley JA, Ensrud K, Browner WS, Nevitt MC, Cummings SR & Osteoporotic Fractures Research Group (2003) BMD at multiple sites and risk of fracture of multiple types: long-term results from the Study of Osteoporotic Fractures. J Bone Miner Res 18(11): 1947–1954.

Trabelsi N, Yosibash Z & Milgrom C (2009) Validation of subject-specific automated p-FE analysis of the proximal femur. J Biomech 42(3): 234–241.

Trabelsi N, Yosibash Z, Wutte C, Augat P & Eberle S (2011) Patient-specific finite element analysis of the human femur--a double-blinded biomechanical validation. J Biomech 44(9): 1666–1672.

Turner C & Burr D (2001) Experimental techniques for bone mechanics. In Cowin S (ed) Bone mechanics handbook. New York, NY, Informa Healthcare.

Turner CH, Rho J, Takano Y, Tsui TY & Pharr GM (1999) The elastic properties of trabecular and cortical bone tissues are similar: results from two microscopic measurement techniques. J Biomech 32(4): 437–441.

Unger S, Blauth M & Schmoelz W (2010) Effects of three different preservation methods on the mechanical properties of human and bovine cortical bone. Bone 47(6): 1048–1053.

van Balen R, Steyerberg EW, Polder JJ, Ribbers TL, Habbema JD & Cools HJ (2001) Hip fracture in elderly patients: outcomes for function, quality of life, and type of residence. Clin Orthop Relat Res (390): 232–243.

Verhulp E, van Rietbergen B & Huiskes R (2008) Load distribution in the healthy and osteoporotic human proximal femur during a fall to the side. Bone 42(1): 30–35.

Vokes TJ, Giger ML, Chinander MR, Karrison TG, Favus MJ & Dixon LB (2006) Radiographic texture analysis of densitometer-generated calcaneus images differentiates postmenopausal women with and without fractures. Osteoporos Int 17(10): 1472–1482.

von Mises R (1913) Mechanik der festen Körper im plastisch deformablen Zustand. Göttin Nachr Math Phys 1: 582–592.

Voo L, Armand M & Kleinberger M (2004) Stress fracture risk analysis of the human femur based on computational biomechanics Johns Hopkins APL Technical Digest 25(3): 223–230.

Wakao N, Harada A, Matsui Y, Takemura M, Shimokata H, Mizuno M, Ito M, Matsuyama Y & Ishiguro N (2009) The effect of impact direction on the fracture load of osteoporotic proximal femurs. Med Eng Phys 31(9): 1134–1139.

Wasnich RD (1997) Epidemiology of osteoporosis in the United States of America. Osteoporos Int 7 Suppl 3: S68–72.

WHO (1994) Assessment of fracture risk and its application to screening for postmenopausal osteoporosis. Report of a WHO Study Group. World Health Organ Tech Rep Ser 843: 1–129.

Willig R, Luukinen H & Jalovaara P (2003) Factors related to occurrence of hip fracture during a fall on the hip. Public Health 117(1): 25–30.

Wolff J (1892) Das Gesetzder transformation der Knochen. Translation by Maquet P & Furlong R (1986) The law of bone remodelling. Springer-Verlag, Berlin.

Zebaze RM, Jones A, Welsh F, Knackstedt M & Seeman E (2005) Femoral neck shape and the spatial distribution of its mineral mass varies with its size: Clinical and biomechanical implications. Bone 37(2): 243–252.

Zethraeus N, Strömberg L, Jönsson B, Svensson O & Öhlén G (1997) The cost of a hip fracture. Estimates for 1,709 patients in Sweden. Acta Orthop Scand 68(1): 13–17.

Zuckerman JD (1996) Hip fracture. N Engl J Med 334(23): 1519–1525.

Zysset PK, Guo XE, Hoffler CE, Moore KE & Goldstein SA (1999) Elastic modulus and hardness of cortical and trabecular bone lamellae measured by nanoindentation in the human femur. J Biomech 32(10): 1005–1012.

Original articles

I Koivumäki J, Thevenot J, Pulkkinen P, Salmi J, Kuhn V, Lochmüller E-M, Link T, Eckstein F & Jämsä T (2010) Does femoral strain distribution coincide with the occurrence of cervical versus trochanteric hip fractures? - An experimental finite element study. Med Biol Eng Comput 48(7): 711–717.

II Koivumäki J, Thevenot J, Pulkkinen P, Kuhn V, Link T, Eckstein F & Jämsä T (2012) CT-based finite element models can be used to estimate experimentally measured failure loads in the proximal femur. Bone 50(4): 824–829.

III Koivumäki J, Thevenot J, Pulkkinen P, Kuhn V, Link T, Eckstein F & Jämsä T (2012) Cortical bone finite element models in the estimation of experimentally measured failure loads in the proximal femur. Bone 51(4): 737–740.

The original articles are not included in the electronic version of the thesis.

Book orders:
Granum: Virtual book store
http://granum.uta.fi/granum/

UNIVERSITY OF OULU P.O.B. 7500 FI-90014 UNIVERSITY OF OULU FINLAND

ACTA UNIVERSITATIS OULUENSIS

ISBN 978-952-62-0090-3 (Paperback)
ISBN 978-952-62-0091-0 (PDF)
ISSN 0355-3221 (Print)
ISSN 1796-2234 (Online)

UNIVERSITY of OULU
OULUN YLIOPISTO